

LOCKHEED MARTIN ENERGY RESEARCH LIBRARIES



CENTRAL RESEARCH LIBRARY  
DOCUMENT COLLECTION

2

3 4456 0513464 5

**NATIONAL LABORATORY**

operated by

**UNION CARBIDE CORPORATION**  
NUCLEAR DIVISION



for the

**U.S. ATOMIC ENERGY COMMISSION**

ORNL - TM - 2023

THE OPTICAL PROPERTIES OF VACUUM-EVAPORATED  
FILMS OF TELLURIUM AND AMORPHOUS SELENIUM  
(Thesis)

J. D. Hayes, Jr.  
E. T. Arakawa  
M. W. Williams

OAK RIDGE NATIONAL LABORATORY  
CENTRAL RESEARCH LIBRARY  
DOCUMENT COLLECTION

**LIBRARY LOAN COPY**

DO NOT TRANSFER TO ANOTHER PERSON

If you wish someone else to see this  
document, send in name with document  
and the library will arrange a loan.

ORNL-700-  
12-2073

Submitted as a thesis by James David Hayes, Jr., to the Graduate School of Vanderbilt University in partial fulfillment of the requirements for the degree of Master of Science in Physics.

#### LEGAL NOTICE

This report was prepared as an account of Government sponsored work. Neither the United States, nor the Commission, nor any person acting on behalf of the Commission:

- A. Makes any warranty or representation, expressed or implied, with respect to the accuracy, completeness, or usefulness of the information contained in this report, or that the use of any information, apparatus, method, or process disclosed in this report may not infringe privately owned rights; or
- B. Assumes any liabilities with respect to the use of, or for damages resulting from the use of any information, apparatus, method, or process disclosed in this report.

As used in the above, "person acting on behalf of the Commission" includes any employee or contractor of the Commission, or employee of such contractor, to the extent that such employee or contractor of the Commission, or employee of such contractor prepares, disseminates, or provides access to, any information pursuant to his employment or contract with the Commission, or his employment with such contractor.

ORNL-TM-2023

Contract No. W-7405-eng-26

HEALTH PHYSICS DIVISION

THE OPTICAL PROPERTIES OF VACUUM-EVAPORATED  
FILMS OF TELLURIUM AND AMORPHOUS SELENIUM

J. D. Hayes, Jr., E. T. Arakawa, and M. W. Williams

Submitted as a thesis by James David Hayes, Jr. to the Graduate School  
of Vanderbilt University in partial fulfillment of the requirements  
for the degree of Master of Science in Physics

JANUARY 1968

OAK RIDGE NATIONAL LABORATORY  
Oak Ridge, Tennessee  
operated by  
UNION CARBIDE CORPORATION  
for the  
U.S. ATOMIC ENERGY COMMISSION



3 4456 0513464 5

## ACKNOWLEDGEMENTS

The authors take great pleasure in expressing their sincere appreciation to: R. D. Birkhoff for his interest and support; R. H. Ritchie and H. C. Schweinler for discussions of the theoretical aspects of this work; R. C. Vehse for his suggestions concerning many techniques employed in this work and for many stimulating discussions of the accuracy of the various methods used to determine the optical constants; J. A. Harter and A. G. Kenerly for assistance in maintaining the apparatus; J. L. Malone and E. T. Loy for their assistance in procuring supplies and completing the drawings; and to Lola Jennings and my wife, Carolyn, for typing the manuscripts.

One of us (J. D. Hayes) would like to express his gratitude to the Atomic Energy Commission for their support of this research and study through its Special Fellowship Program in Health Physics which is administered by the Oak Ridge Associated Universities.

## TABLE OF CONTENTS

	Page
ACKNOWLEDGEMENTS . . . . .	ii
LIST OF FIGURES . . . . .	v
Chapter	
I. INTRODUCTION . . . . .	1
II. THEORY. . . . .	4
III. EXPERIMENTAL APPARATUS . . . . .	8
A. General Apparatus . . . . .	8
B. Light Source . . . . .	8
C. Monochromator . . . . .	11
D. Vacuum Systems . . . . .	12
E. Current Measuring Equipment . . . . .	13
F. Reflectance Chamber . . . . .	13
IV. EXPERIMENTAL PROCEDURE. . . . .	16
A. Spectrometer Alignment and Calibration . . . . .	16
B. Film Preparation . . . . .	18
C. Reflectance Measurements . . . . .	18
D. Determination of the Polarization of the Incident Light . . . . .	18
E. Transmission Measurements . . . . .	19
F. Critical Angle Measurements . . . . .	21

TABLE OF CONTENTS (Continued)	Page
V. DATA REDUCTION . . . . .	23
VI. RESULTS AND CONCLUSIONS . . . . .	38
A. Selenium . . . . .	38
B. Tellurium . . . . .	43
LIST OF REFERENCES. . . . .	50

## LIST OF FIGURES

Figure	Page
1. Schematic Diagram of Light Source, Spectrometer, and Reflectance Chamber. . . . .	9
2. Schematic Drawing of Condensed-Spark-Discharge Light Source . . . . .	10
3. Reflectance Chamber . . . . .	14
4. Polarization of Incident Light . . . . .	20
5. Reflectance of Amorphous Selenium as a Function of Energy for 20°, 45°, and 70° Angles of Incidence . . . . .	24
6. Optical Constants of Selenium Obtained from Two-Angle Method . . . . .	25
7. Input Reflectance for Dispersion Analysis of Selenium . . . . .	28
8. $\Delta\phi(E_o)$ versus $E_o$ for Selenium . . . . .	29
9. Optical Constants of Selenium versus Energy . . . . .	31
10. Transmission of Tellurium Films versus Thickness. . . . .	32
11. Comparison of Optical Constants of Tellurium Obtained by the Various Methods Described in the Text. . . . .	34
12. Input Reflectance for Dispersion Analysis of Tellurium . . . . .	35
13. $\Delta\phi(E_o)$ versus $E_o$ for Tellurium. . . . .	36
14. Optical Constants of Tellurium versus Energy. . . . .	37
15. Dielectric Constants of Selenium versus Energy. . . . .	40
16. The Energy Loss Functions of Selenium versus Energy . . . . .	42
17. Reflectance of Vacuum-evaporated Tellurium as a Function of Energy for 20°, 45°, and 75° Angles of Incidence. . . . .	44
18. Dielectric Constants of Tellurium versus Energy . . . . .	47
19. The Energy Loss Functions of Tellurium versus Energy. . . . .	48



## CHAPTER I

### INTRODUCTION

The optical constants of a material yield much information about the energy absorption processes which take place when ionizing radiation is incident on the material, and this information is useful in establishing the band structure of the material and energy absorption cross sections. Recent improvements in vacuum ultraviolet equipment, particularly light sources, grating and detectors, have made it possible to determine more accurately the optical constants of solids in the energy region from 6 eV to 25 eV. This region is of interest because of the many energy absorption processes which take place in this energy interval, such as interband transitions, the generation of excitons, and collective oscillations of electrons.

Because most materials are highly absorbing in the vacuum ultraviolet and because of a lack of good polarizers for this region, the optical properties in the vacuum ultraviolet are generally determined by reflectance techniques. The two most common methods are the dispersion analysis, or Kramers-Kronig analysis,<sup>1,2</sup> and the "two-angle method." The two-angle method requires the measurement of the reflectance, at two different angles of incident, of unpolarized light or of light of known polarization. Using these values of the reflectance it is then possible to solve the Fresnel reflection equations for the real and imaginary parts of the complex index of refraction. From these quantities the real and

imaginary parts of the complex dielectric constant and the volume and surface-plasma loss functions can be calculated. The dispersion analysis method requires the measurement of the reflectance at normal or near-normal incidence over a large energy interval. The phase shift upon reflection is then calculated using the dispersion relations and from this shift the optical constants can be calculated.

Still another method for determining the real part of the complex refractive index from reflectance measurements is the critical-angle method.<sup>3</sup> This method is based on the fact that if the extinction coefficient of a material is small, there is a rapid increase in reflectance for angles of incidence near the critical angle, the angle which marks the onset of total reflection. The advantage of this method is that it can be used when the normal incidence reflectance of a material is very small. Since the extinction coefficient must be small in order to use this method to determine the real part of the complex refractive index, the imaginary part can be determined by transmission measurements.

Both the two-angle method and the Kramers-Kronig analysis were used in this work to obtain the optical constants of selenium and tellurium since the two-angle method was good at higher energies but not sensitive enough at the lower energies while the Kramers-Kronig method was well-suited to the lower energies but not so accurate at the higher energies. In addition the critical-angle method was used in conjunction with transmission measurements to determine the optical constants of tellurium above 18 eV where the reflectance was low.

The primary purpose of this work was to obtain accurate optical constants for vacuum-evaporated selenium and tellurium films for the

ultraviolet spectral region. The optical constants were used to calculate the real and imaginary parts of the complex dielectric constant and the volume and surface-plasma energy loss functions.

There has been some previous work on the optical constants of selenium in the wavelength region investigated in this study. However, the previous work was done on films which had been exposed to air. S. Robin-Kandare<sup>4,5</sup> has measured the transmission of selenium films in the spectral region 110 Å to 4000 Å and the reflectance of selenium in the spectral region 550 Å to 1500 Å. W. L. Goffe and M. P. Givens<sup>6</sup> have measured the reflectance of selenium in the spectral region 550 Å to 1500 Å. The reflectance of our films was higher than that of previous investigators and the structure was more pronounced. The differences are probably due to differences in the quality of the films studied.

The reflectance of polycrystalline tellurium films on amorphous substrates has been measured by several workers<sup>7,8,9,10</sup> for the energy region above 3 eV. Their values differ in magnitude and shape and are significantly lower than those measured in this work. S. Robin-Kandare,<sup>8</sup> Rustgi,<sup>9</sup> and Merdy<sup>10</sup> have made transmission measurements on polycrystalline tellurium films in the ultraviolet spectral region. The discrepancies between their results and those of the present work are also attributed to differences in the quality of the films studied. Great care was taken in this work to prepare films of high quality and to obtain reproducible results.

## CHAPTER II

### THEORY

The optical properties of absorbing media may be described quantitatively by the complex refractive index,  $N = n + ik$ , where  $n$ , the real part of the refractive index, is defined as the ratio of the velocity of light in vacuum ( $c$ ) to the phase velocity ( $v$ ) in the dielectric of a plane electromagnetic wave having constant amplitude along a wave front,

$$n = c/v \quad (1)$$

The imaginary part of the complex refractive index,  $k$ , often called the extinction coefficient, describes the damping of the wave as it traverses the absorbing medium, and is defined by the relation

$$E = E_0 \exp \left( - \frac{2 \pi k z}{\lambda} \right) \quad (2)$$

where  $z$  is the coordinate in the direction of propagation,  $E_0$  is the amplitude of the electromagnetic wave at  $z = 0$ ,  $E$  is the amplitude at  $z$ , and  $\lambda$  is the wavelength in vacuum of the electromagnetic wave.

The theory of reflection and transmission of light by thin films has been discussed in many texts.<sup>2,11,12,13</sup> Expressions for the reflectance ( $R$ ) at a given wavelength are obtained by the application of boundary conditions to Maxwell's equations for a plane electromagnetic wave incident on the boundary between two media. For an infinitely thick absorbing film the equations for the components of the reflected light

are given by the Fresnel equations:

$$R_s = \left| \left| \frac{[(n+ik)^2 - \sin^2 \theta]^{\frac{1}{2}} - \cos \theta}{[(n+ik)^2 - \sin^2 \theta]^{\frac{1}{2}} + \cos \theta} \right| \right|^2 \quad (3)$$

$$R_p = \left| \left| \frac{[(n+ik)^2 - \sin^2 \theta]^{\frac{1}{2}} - (n+ik)^2 \cos \theta}{[(n+ik)^2 - \sin^2 \theta]^{\frac{1}{2}} + (n+ik)^2 \cos \theta} \right| \right|^2 \quad (4)$$

where  $R_s$  and  $R_p$  are the reflectances for light with the electric field vector perpendicular and parallel respectively to the plane of incidence and  $\theta$  is the angle of incidence.

For unpolarized light, for light polarized at  $45^\circ$  to the plane of incidence, and for circularly polarized light the reflectance ( $R$ ) is given by

$$R = \frac{1}{2} (R_s + R_p) \quad (5)$$

For partially plane polarized light the reflectance is given by<sup>14</sup>

$$R = (PR_p + R_s) / (1 + P) \quad (6)$$

where the parameter  $P$  is defined by the relation

$$P = \frac{I_p}{I_s} \quad (7)$$

with  $I_p$  and  $I_s$  being the intensities of the incident light with the electric field vector parallel and perpendicular, respectively, to the plane of incidence of the sample.

If  $P$  is known and  $R$  is measured for two angles of incidence, then Equations (3), (4) and (6) constitute a system of equations which can be solved by graphical or numerical methods to yield the optical constants

n and k.

The reflectance,  $R(E)$ , can be expressed in terms of  $\tilde{r}(E)$ , the complex reflectance amplitude, by:

$$R(E) = \tilde{r}(E)^* \tilde{r}(E) = |\tilde{r}(E)|^2 \quad (8)$$

For normal incidence the complex reflectance amplitude,  $\tilde{r}(E)$ , is given by

$$\tilde{r}(E) = r(E) e^{-i\phi(E)} = \frac{n+ik-1}{n+ik+1} \quad (9)$$

The magnitude  $r(E)$  and the phase  $\phi(E)$  are not completely independent.

They are related by the phase shift dispersion relation

$$\phi(E_0) = \frac{E_0}{\pi} \int_0^{\infty} \frac{\ln R}{E^2 - E_0^2} dE \quad (10)$$

$\phi(E_0)$  is restricted to the range  $-\pi \leq \phi \leq 0$ .

The optical constants n and k are determined from  $\phi(E)$  and  $R(E)$  by the relations

$$n = \frac{1 - R}{1 + R - 2\sqrt{R} \cos \phi} \quad (11)$$

$$k = \frac{-2\sqrt{R} \sin \phi}{1 + R - 2\sqrt{R} \cos \phi} \quad (12)$$

Another useful relation is

$$\tan \phi = \frac{-2k}{n^2 + k^2 - 1} \quad (13)$$

Thus, if the normal or near-normal incidence reflectance is known over a wide enough energy range, the phase shift and therefore the optical constants can be calculated in the region where the reflectance is known.

The advantage of this method over other reflectance methods of determining optical constants is that measurements may be made near normal incidence, and the polarization of the incident light need not be known. There are several disadvantages. One is that the reflectance must be known over such a wide energy range that some extrapolation technique generally must be used beyond the region where data is available. Another is that errors in the reflectance measurement at one energy will affect the calculated optical constants at all energies.

The complex dielectric constant,  $\epsilon = \epsilon_1 + i \epsilon_2$ , is related to the complex refractive index by  $\epsilon = N^2$  so that

$$\epsilon_1 = n^2 - k^2 \quad (14)$$

$$\epsilon_2 = 2nk \quad (15)$$

The volume and surface-plasma loss functions are given by  $-\text{Im} \left( \frac{1}{\epsilon} \right)$  and  $-\text{Im} \left( \frac{1}{\epsilon+1} \right)$ , respectively.

The optical properties are specified when these factors are known as a function of incident photon energy.

## CHAPTER III

### EXPERIMENTAL APPARATUS

#### A. General Description

The apparatus, depicted schematically in Figure 1, consisted primarily of a light source and detector, a scanning monochromator, a reflectance chamber, current measuring instruments, and vacuum systems.

Light from the source passed into the monochromator through the entrance slit and filter assembly and was incident on the grating. Light of the selected wavelength passed from the grating through the exit slit into the reflectance chamber and on to the evaporated film. The light intensities were detected by a photomultiplier tube which was rotated about the vertical axis of the sample. The output from the photomultiplier tube was measured by a pico-ammeter and recorded by a Minneapolis-Honeywell Brown recorder. The monochromator and the reflectance chamber were evacuated by separate vacuum systems.

#### B. Light Source

The capillary discharge light source used is depicted schematically in Figure 2, and consisted of a boron nitride cylinder and a water-cooled brass anode and cathode. This source was mounted on a  $\frac{1}{2}$ " brass spacer ring which in turn was mounted on the entrance slit assembly. A Hastings model DV-4DM thermocouple gage, mounted in the spacer ring, was used to measure the pressure in the light source. A  $\frac{1}{4}$ " vacuum line from the

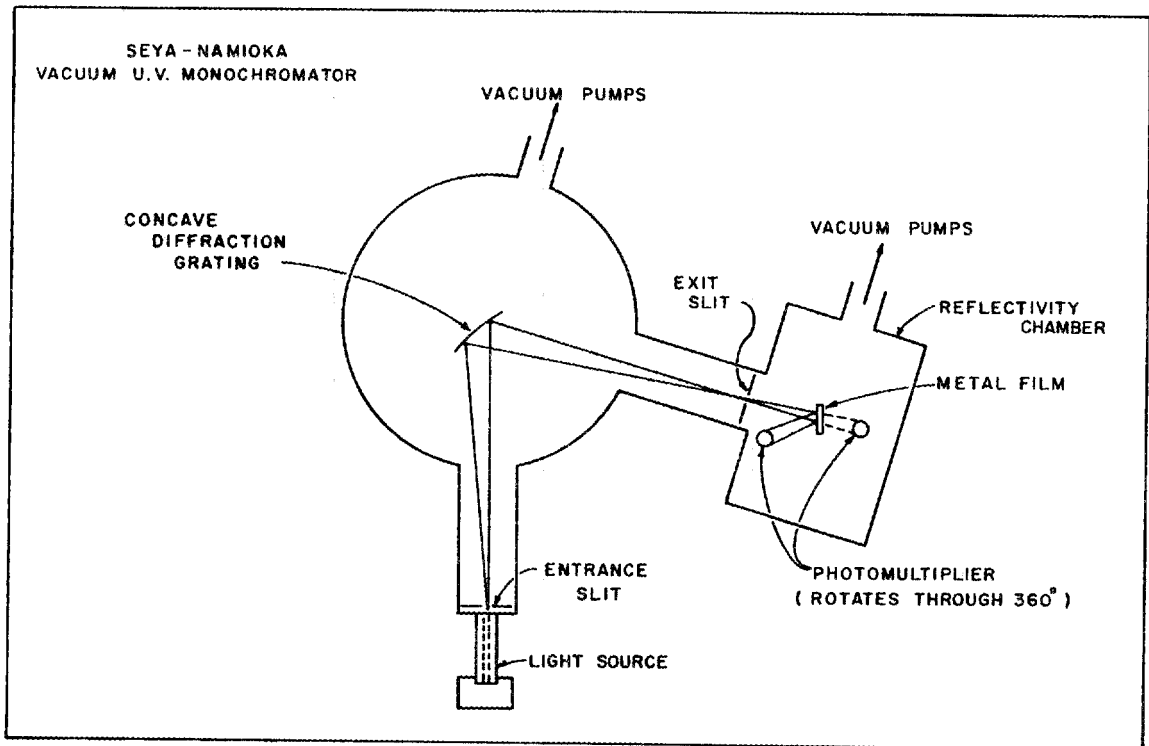


Fig. 1. Schematic Diagram of Light Source, Spectrometer and Reflectance Chamber.

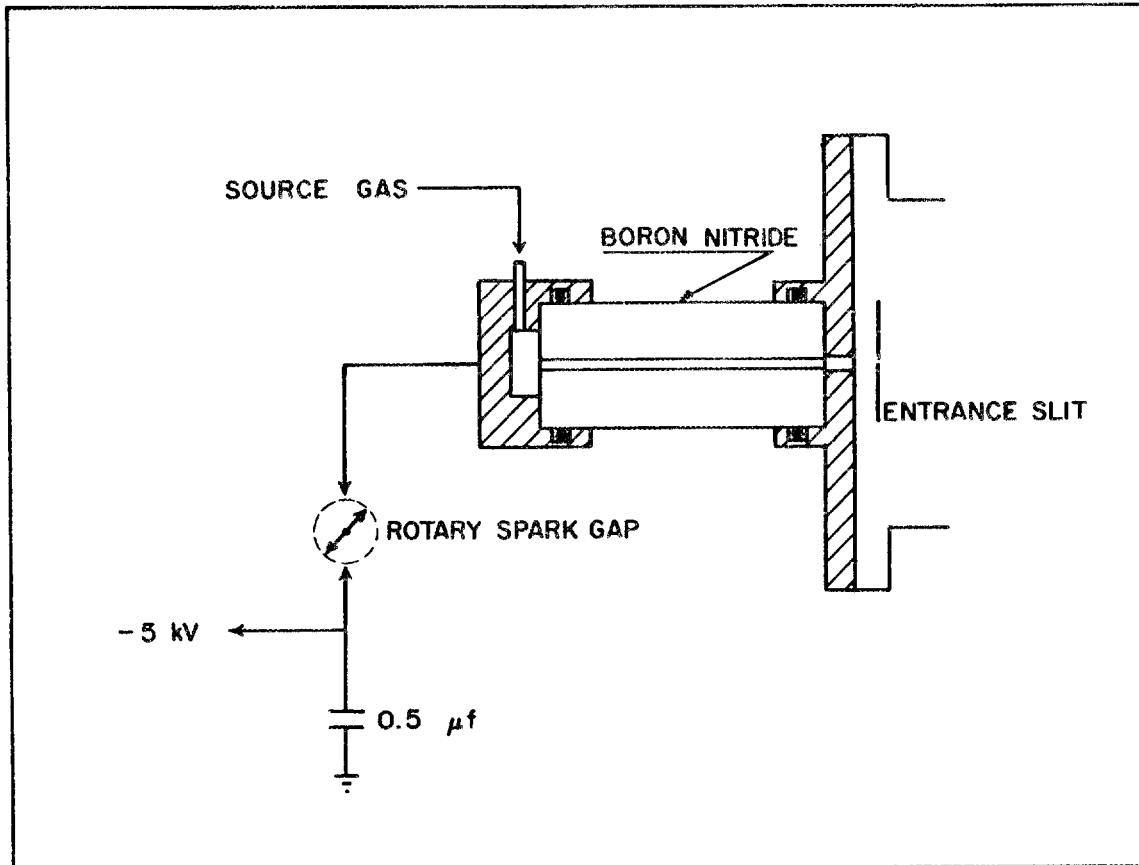


Fig. 2. Schematic Drawing of Condensed-Spark-Discharge Light Source.

forepump to the space between the light source and the entrance slit was used to evacuate the light source. The discharge gas was leaked slowly into the capillary tube at the anode by means of a needle valve. The light source could be operated in either of two modes, d. c. arc discharge or spark discharge. The spark discharge mode was used for wavelengths below  $1500 \text{ \AA}$  while the d. c. arc discharge mode was used for wavelengths between  $1500 \text{ \AA}$  and  $4000 \text{ \AA}$ . High voltage for the discharge was supplied by a Consolidated Vacuum LC-031 power supply. Typical operating conditions in the d. c. arc mode were a current of 250 milliamperes at 600 volts with a light source pressure of 1000 microns Hg. A rotating spark gap with a repetition rate of 56 pulses per second was used to discharge a  $0.5 \mu\text{f}$  capacitor through the light source in the spark mode. Typical operating conditions in the spark mode were a current of 150 milliamperes at 5000 volts with a light source pressure of 400 microns Hg.

The stability of the light source was very sensitive to changes in the light source pressure and to the condition of the spark gap when operating in the air spark discharge mode. The spark gap had to be adjusted each time prior to use to obtain maximum stability, and the "O" rings in the light source had to be changed often since the heat dissipated in the boron-nitride cylinder dried them out rapidly.

### C. Monochromator

A 0.5 meter Seya-Namioka type vacuum scanning monochromator built at ORNL was used to select the incident radiation. The bilateral entrance and exit slits were continuously adjustable from 10 microns to 6

millimeters by means of rotating shafts extending through the housing. Each slit assembly incorporated a slide valve which made it possible to isolate the monochromator from the light source and the reflectance chamber.

The diffraction grating used was a Bausch and Lomb concave grating with a 0.5 meter radius of curvature. The grating was ruled with six hundred lines per mm. with a 1500 Å blaze and was coated with aluminum and overcoated with magnesium fluoride ( $MgF_2$ ).

#### D. Vacuum Systems

A National Research Corporation (NRC) model HS6-1500 six-inch water-cooled oil diffusion pump, with a pumping speed of 1400 liters per second at  $10^{-6}$  Torr, backed by a Welch model 1397 rotary forepump was connected to the reflectance chamber through a NRC water-cooled baffle, a NRC slide valve and an elbow flange. Pressure in the reflectance chamber was measured by a Veeco RG 75K ionization gage tube and read on a Vacronic ion gage control model SP-230.

A similar system with two exceptions was used to evacuate the monochromator. The diffusion pump used was a NRC VHS6 six-inch water-cooled oil diffusion pump with a pumping speed of 2400 liters per second at  $10^{-6}$  Torr, and the slide valve was connected directly to the monochromator.

The reflectance chamber could be isolated from the monochromator by means of a slide valve incorporated in the exit slit assembly.

### E. Current Measuring Equipment

The incident and reflected light intensities were measured by means of a RCA 1P28 photomultiplier tube equipped with a sodium salicylate wavelength converter. The operating voltage of 540 volts was supplied by a regulated power supply built at ORNL. The output from the photomultiplier tube was integrated using an RC circuit and was measured on a Keithley Model 409 pico-ammeter and recorded by a Minneapolis-Honeywell Brown 10 millivolt recorder. The range of photocurrents measured was  $10^{-7}$  to  $10^{-11}$  amperes. The pico-ammeter and the recorder were calibrated with a Keithley model 261 standard current source.

### F. Reflectance Chamber

The chamber used for preparing and measuring the reflectance of the films is illustrated in Figure 3.

The evaporated film, film holder, evaporation boat, and the light detector were enclosed in a stainless steel cylinder 16 inches long and  $8\frac{1}{2}$  inches in diameter with vacuum and viewing ports. One port of the cylinder was connected by an elbow flange to a vacuum pump. The opposite port was connected by a stainless steel yoke to the exit slit of the monochromator. Vacuum seals were accomplished by Viton "O" rings. The cylinder was mounted in a vertical position with the vacuum ports at the lower half of the cylinder. The entire cylinder was electro-polished inside and outside.

The top portion of the cylinder contained the high current feed-throughs, the baffle and shutter assembly, and the sample holder assembly.

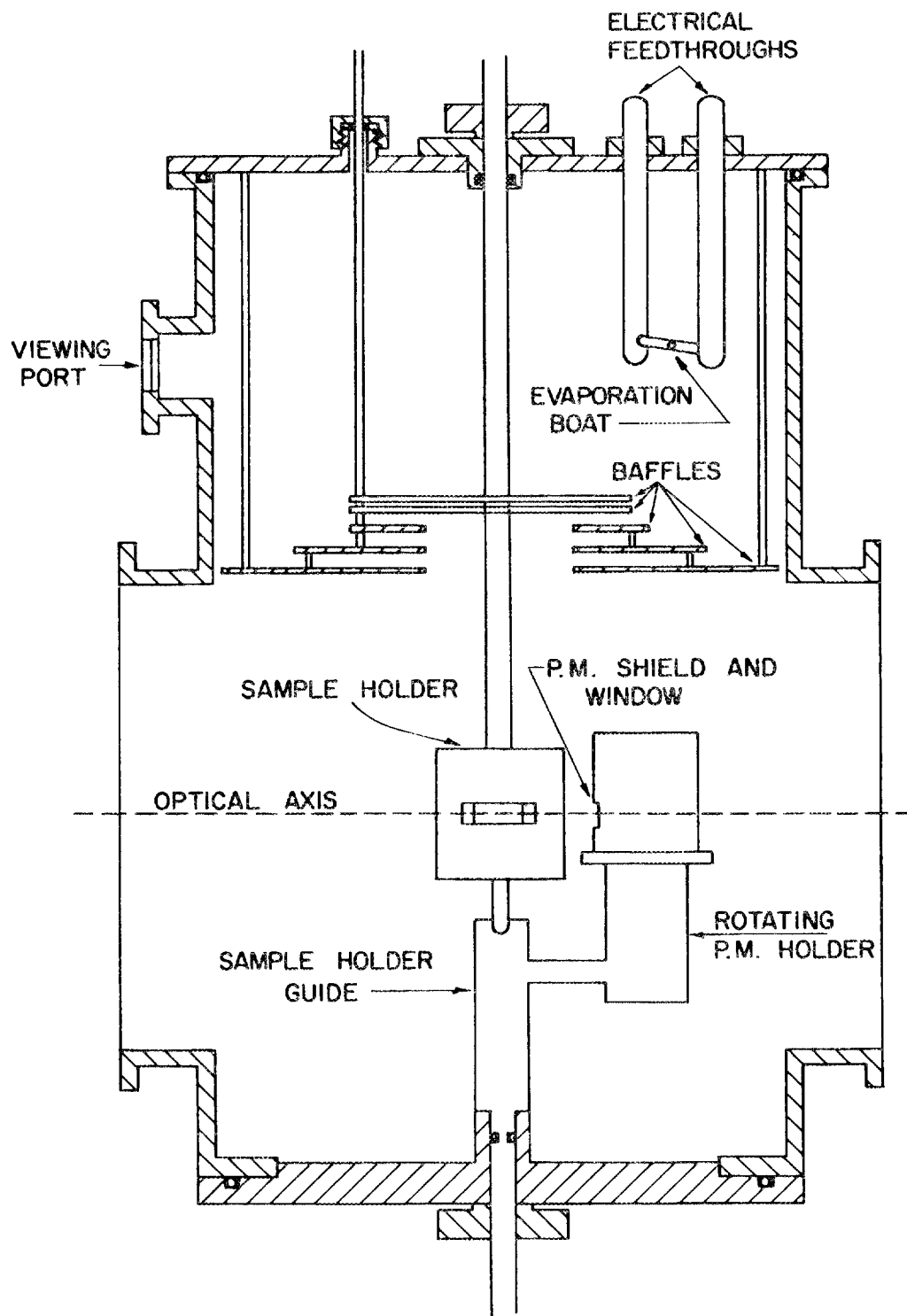


Fig. 3. Reflectance Chamber.

The sample holder guide and the rotating photomultiplier tube holder were mounted on the base of the cylinder. The sample holder was designed for vertical positioning and independent angular rotation about an axis normal to the plane of incidence by a shaft extending through the vacuum system. This permitted the positioning of the sample film at various angles of incidence when measurements of the reflected light were made, or withdrawal from the beam to allow measurement of the incident intensity. The detector was rotated about the same axis as the sample holder by a similar arrangement.

For evaporation, the sample holder containing a clean slide was raised into the upper part of the chamber and the baffle shutter closed. The sample was evaporated onto the slide from the tubular boat mounted on the electrical feedthroughs. The evaporation process could be observed through viewing ports in the upper section.

The reflectance measurements were made in the lower section of the chamber.

## CHAPTER IV

### EXPERIMENTAL PROCEDURE

#### A. Spectrometer Alignment and Calibration

The initial alignment of the spectrometer consisted of centering the grating face on the grating table, adjusting the tilt and level of grating, focusing the spectrometer with the entrance and exit slits equidistant from the grating, and aligning the entrance and exit slits parallel with the rulings on the grating. Optical stops were placed in the entrance and exit arms to confine the beam area at the sample to approximately  $5 \text{ mm}^2$  at normal incidence.

The spectrometer was calibrated using known spectral lines in the air spark and air d. c. arc spectra.

#### B. Film Preparation

The films used in this experiment were prepared by vacuum evaporation in the upper half of the reflectance chamber. The boats used to evaporate the selenium were made from stainless steel tubing .005" in thickness and were cleaned by soaking in a sulfuric acid-sodium dichromate solution followed by rinsing in running distilled water for an hour. The boats were dried with compressed air and mounted on the current feed-throughs in the reflectance chamber.

A predetermined amount of selenium or tellurium was placed in the tubular boat and the top of the reflectance chamber was then mounted in

place, and the sample holder was aligned with the monochromator. The selenium and tellurium used had a specified purity of 99.999% and were obtained from the United Mineral and Chemical Corporation.<sup>15</sup>

The glass microscope slides used as substrates were subjected to an extensive cleaning procedure. The slides were soaked overnight in Knox-60<sup>16</sup> cleaning solution, then rinsed in running distilled water for an hour, soaked in a sulfuric acid-sodium dichromate solution for half an hour, then rinsed again in running distilled water for an hour, and, finally, placed in an isopropyl alcohol degreaser for half an hour. The alcohol treatment removed all traces of grease, and upon removal from the degreaser the slides were hot and dried immediately. Since the slides were hot, the chance of water vapor from the air condensing on the slides was small. A clean slide was immediately placed in the sample holder and the system pumped down.

The distance from the evaporation boat to the substrate was 9 cm. Vacuums of the order of  $10^{-6}$  Torr were maintained during the evaporations, and the pressure in the reflectance chamber was never over  $6 \times 10^{-6}$  Torr while taking data for selenium and  $2 \times 10^{-5}$  Torr for tellurium.

The substrate was positioned so that it was shielded from the boat until the boat and the sample were outgassed. The substrate was then exposed to the boat and the current increased. The evaporation took place over a period of about 3 seconds. Typical film thicknesses were 3000 Å to 6000 Å.

### C. Reflectance Measurements

Both the film and the photomultiplier could be rotated to permit reflectance measurements to be obtained at several different angles of incidence. The photomultiplier was positioned manually for peak intensities. The reflectance at  $20^\circ$ ,  $45^\circ$ , and  $70^\circ$  was measured using known spectral lines with air or argon as the source gas.

The primary components of the background were phototube dark current and scattered light. Lithium fluoride, quartz, and glass filters were used to determine the background intensity as a function of wavelength and to eliminate second order diffraction of the short wavelength lines from the spectral regions covered. The background in the spark mode was found to be constant for wavelengths above  $200 \text{ \AA}$ , while the background in the d. c. arc mode was constant above  $500 \text{ \AA}$ , for a given phototube position. These constant background intensities were measured for each phototube position and subtracted from the corresponding intensities measured at each spectral line used.

### D. Determination of the Polarization of the Incident Light

Since the grating is known to polarize the incident light considerably in the Seya geometry, it was necessary to determine the polarization of the light incident on the sample.

This polarization, P, was measured using a reflection type polarizer consisting of three mirrors of evaporated gold with angles of incidence of  $75^\circ$ ,  $60^\circ$ , and  $75^\circ$ . This polarizer has been described elsewhere.<sup>14</sup> The polarizer was attached to the exit arm of the monochromator and

aligned so that the emerging beam was not deflected as the mirrors were rotated. A photomultiplier tube coated with sodium salicylate was connected to the exit side of the polarizer. Two intensity measurements were made for each spectral line used: one,  $I_p^m$ , with the grating and polarizer having a common plane of incidence and the others,  $I_s^m$ , with the polarizer plane of incidence perpendicular to the grating plane of incidence. The polarization introduced by the polarizer,  $q$ , was calculated using published values of  $n$  and  $k$  for gold.<sup>17</sup> The polarization,  $P$ , of the light emerging from the monochromator was then determined using the relation<sup>14</sup>

$$P = \frac{I_p^m - qI_s^m}{I_s^m - qI_p^m} \quad (16)$$

The degree of polarization of the light incident on the sample using the 1500 Å blaze grating in this experiment is shown versus energy in Figure 4.

#### E. Transmission Measurements

Thin aluminum foils were prepared by evaporating aluminum onto microscope slides coated with a wetting agent,<sup>18</sup> and then immersing the slides slowly into distilled water to float off the aluminum foils. The aluminum foils were picked up on stainless steel holders having circular apertures about 1 cm. in diameter so that the foils covered the apertures. These holders were then mounted on the sample holder in the reflectance chamber so that the incident beam was incident normally on the aluminum

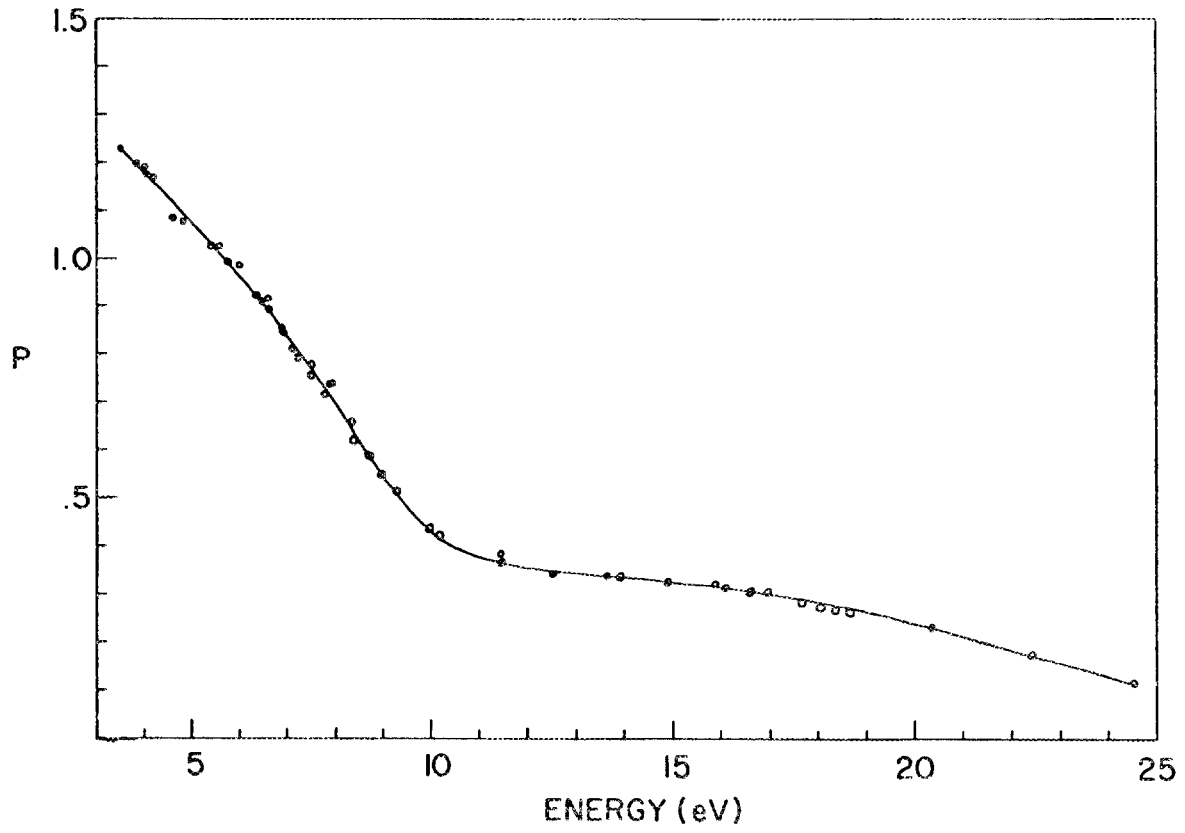


Fig. 4. Polarization of Incident Light.

foils. The foils could be moved to allow for measurements of the incident light intensity without moving the phototube.

The transmission of the aluminum foils was measured and the foils removed from the reflectance chamber and mounted on the ends of clean glass microscope slides at various distances from a stainless steel tubular boat containing tellurium. The tellurium was evaporated onto the aluminum foils and glass slides at a pressure of  $2 \times 10^{-5}$  Torr.

The transmission of the tellurium-coated aluminum foils was then measured in the reflectance chamber with the foils in the same geometry as before. The tellurium films on the microscope slides to which the aluminum foil holders were mounted during evaporation were overcoated with silver, and the thicknesses of these tellurium films were determined interferometrically.

#### F. Critical Angle Measurements

The critical angle method for determining the refractive index is based on the fact that if the extinction coefficient of a material is small, there is a rapid increase in reflectance for angles of incidence near the critical angle, the angle which marks the onset of total reflection. Hunter<sup>3</sup> has discussed the use of this method for determining the real part of the complex refractive index. His calculations show that the angle at which the slope of the curve of the reflectance as a function of angle of incidence is a maximum can be used as an approximate value of the critical angle. The reflectance was measured as a function of angle of incidence utilizing an electric-motor-driven sample holder connected to

the phototube through a belt-drive angle-doubler system so that the phototube was always at an angle which was twice the angle of incidence.

## CHAPTER V

### DATA REDUCTION

The primary data were corrected for background as described in chapter IV, and the reflected intensities plotted. A typical set of reflectance curves for amorphous selenium is shown in Figure 5. Equations (3) and (4) were used to calculate the constants  $n$  and  $k$  by means of a computer program written for the CDC 1604-A computer at the Oak Ridge National Laboratory using values of reflectance taken from the curves drawn through the experimental data. The computer program utilizes Newton's method of successive approximations and corrects for the polarization of the incident light by the use of Equation (6).

The initially assumed values of  $n$  and  $k$  in the iterative process were obtained using the charts published by Ishiguro and Sasaki.<sup>19</sup> These charts consist of curves for constant values of  $n$  and  $k$  plotted for reflectance at  $20^\circ$  incidence (abscissa) and reflectance at  $70^\circ$  incidence (ordinate). The values obtained from these curves were sufficiently accurate for the initial guesses.

Since the reflectance was measured at three angles of incidence,  $20^\circ$ ,  $45^\circ$ , and  $70^\circ$ , three different sets of values of  $n$  and  $k$  were computed and compared. This gave a check on the consistency of the input reflectances. Typical results for  $n$  and  $k$  for selenium are shown in Figure 6.

For selenium the two angle method gave quite consistent results

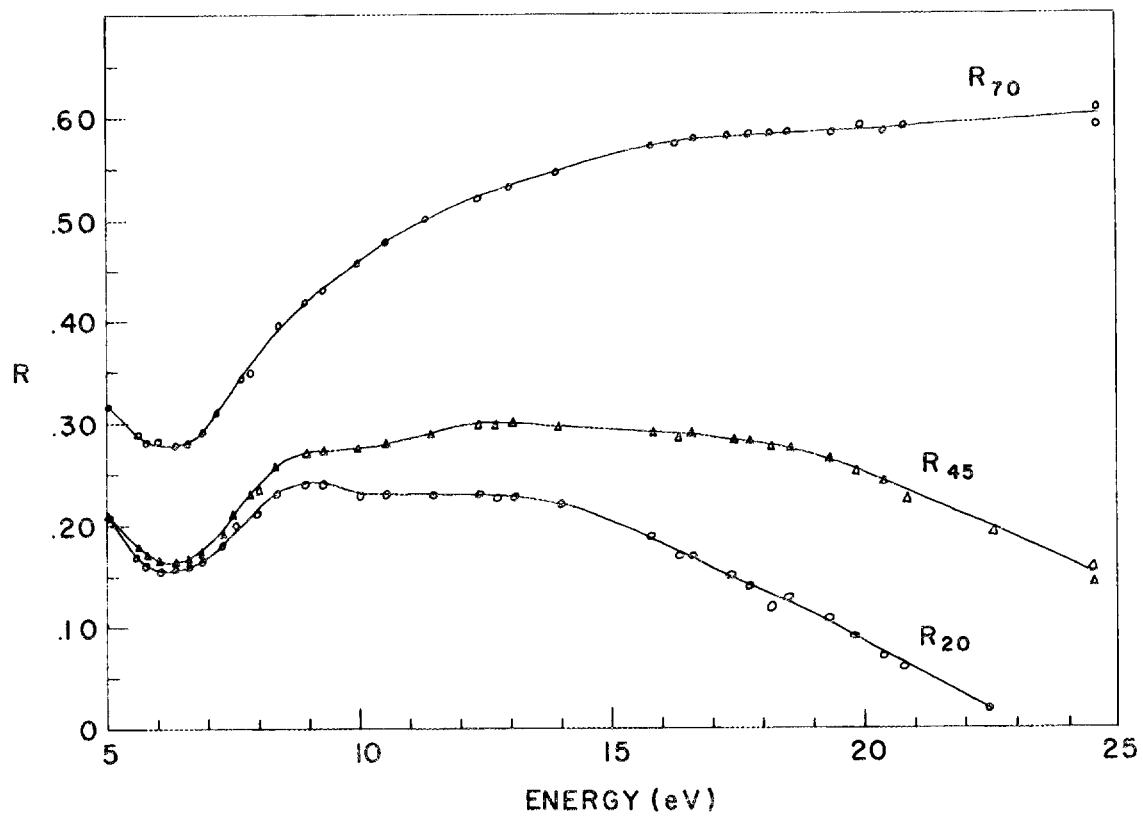


Fig. 5. Reflectance of Amorphous Selenium as a Function of Energy for 20°, 45°, and 70° Angles of Incidence.

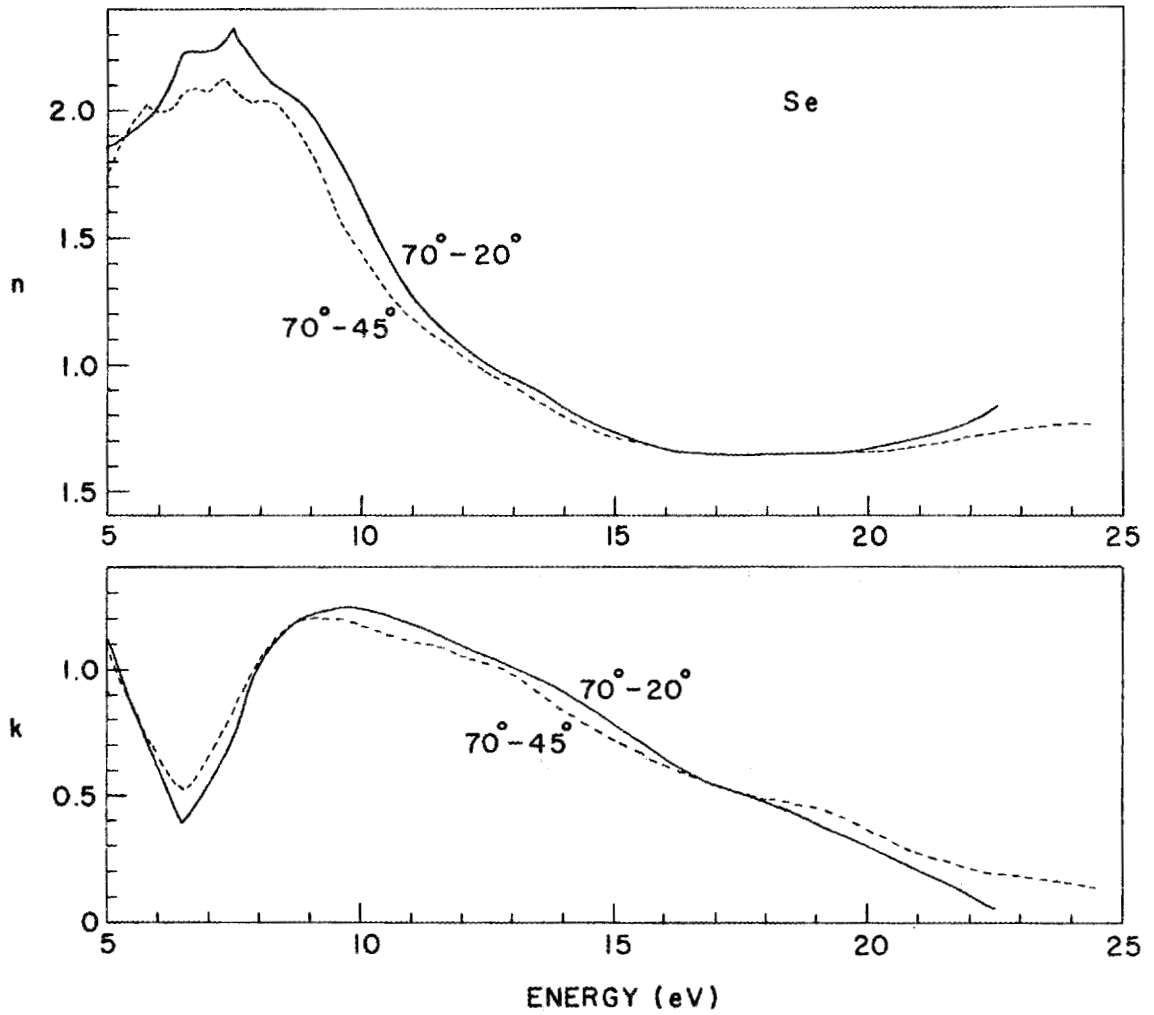


Fig. 6. Optical Constants of Selenium Obtained from Two-Angle Method.

for the optical constants in the region above about 15 eV, as can be seen in Figure 6, but the consistency was not very good for energies below about 12 eV. Hunter<sup>20</sup> has discussed the errors in the two angle method. His analysis shows that in general when  $n$  and  $k$  are large (greater than 1), a small error in the reflectance or polarization can result in large uncertainties in  $n$  or  $k$ , especially for incident light polarized perpendicular to the plane of incidence. Above 10 eV, the incident light was largely polarized perpendicular to the plane of incidence (Figure 4), and up to about 13 eV the constants  $n$  and  $k$  for selenium were large (Figure 6). Therefore, discrepancies could be expected in the results from the two angle method for energies below 13 eV for selenium. Above 13 eV,  $n$  and  $k$  were small and good results from the two-angle method is expected.

Since the two-angle method gave discrepancies at the lower energies, we decided to use the dispersion-analysis method also. This method is useful when data over a wide energy range is available. The principle disadvantages of this method were listed in Chapter II. For selenium, good data<sup>21,22,23</sup> were available for energies up to 5 eV (see comments page 2). However, the optical constants in the energy region from 5 to 15 eV obtained from the dispersion analysis depend to a large extent on the extrapolation used above the last data points. Various extrapolation procedures have been used with good success by other workers.<sup>24,25,26</sup> However, for this work, since good data exist below 5 eV and since the two-angle method gave good results above 15 eV, the phase change on reflection,  $\phi(E_0)$ , could be calculated in these regions from Equation (13). Then Equation (10) can be written

$$\begin{aligned}
\phi(E_0) &= \frac{E_0}{\pi} \int_0^{\infty} \frac{\ln R}{E^2 - E_0^2} dE \\
&= \frac{E_0}{\pi} \int_0^{E_c} \frac{\ln R}{E^2 - E_0^2} dE + \frac{E_0}{\pi} \int_{E_c}^{\infty} \frac{\ln R}{E^2 - E_0^2} dE \\
&= \frac{E_0}{\pi} \int_0^{E_c} \frac{\ln R}{E^2 - E_0^2} dE + \Delta\phi(E_0)
\end{aligned} \tag{17}$$

For selenium the integral for 0 to  $E_c$  eV was evaluated numerically using the 20° reflectance values from the present work up to 22.5 eV and values calculated from the data of Vasko,<sup>21</sup> Caldwell and Fan,<sup>22</sup> and Koehler, et. al.<sup>23</sup> (0.2 eV to 5 eV) utilizing a computer program written for the CDC 1604-A computer at the Oak Ridge National Laboratory. A graph of the input reflectance is shown in Figure 7. The phase change on reflection,  $\phi(E_0)$ , was calculated for several energies  $E_0$  for which the constants  $n$  and  $k$  were known and the corresponding phase change values given by the integral from 0 to 22.5 eV subtracted from these values. This gave values for  $\Delta\phi(E_0)$ , the contribution to the phase change on reflection due to absorption in the energy region above 22.5 eV. Values of  $\Delta\phi(E_0)$  plotted versus energy are shown in Figure 8.  $\Delta\phi(E_0)$  was interpolated in the energy region 4 to 17 eV by a smoothly varying curve as shown by the curve in Figure 8. This method was first used by MacRae, Arakawa, and Williams<sup>27</sup> for tin. For selenium this curve is very nearly that which one obtains using the extrapolation method suggested by Roessler.<sup>25</sup> Values of  $\Delta\phi(E_0)$  in the energy region 2 to 17 eV obtained from this curve were substituted back into Equation (17) to obtain values of  $\phi(E_0)$ . These values along with the reflectance  $R(E_0)$  were used to calculate  $n$

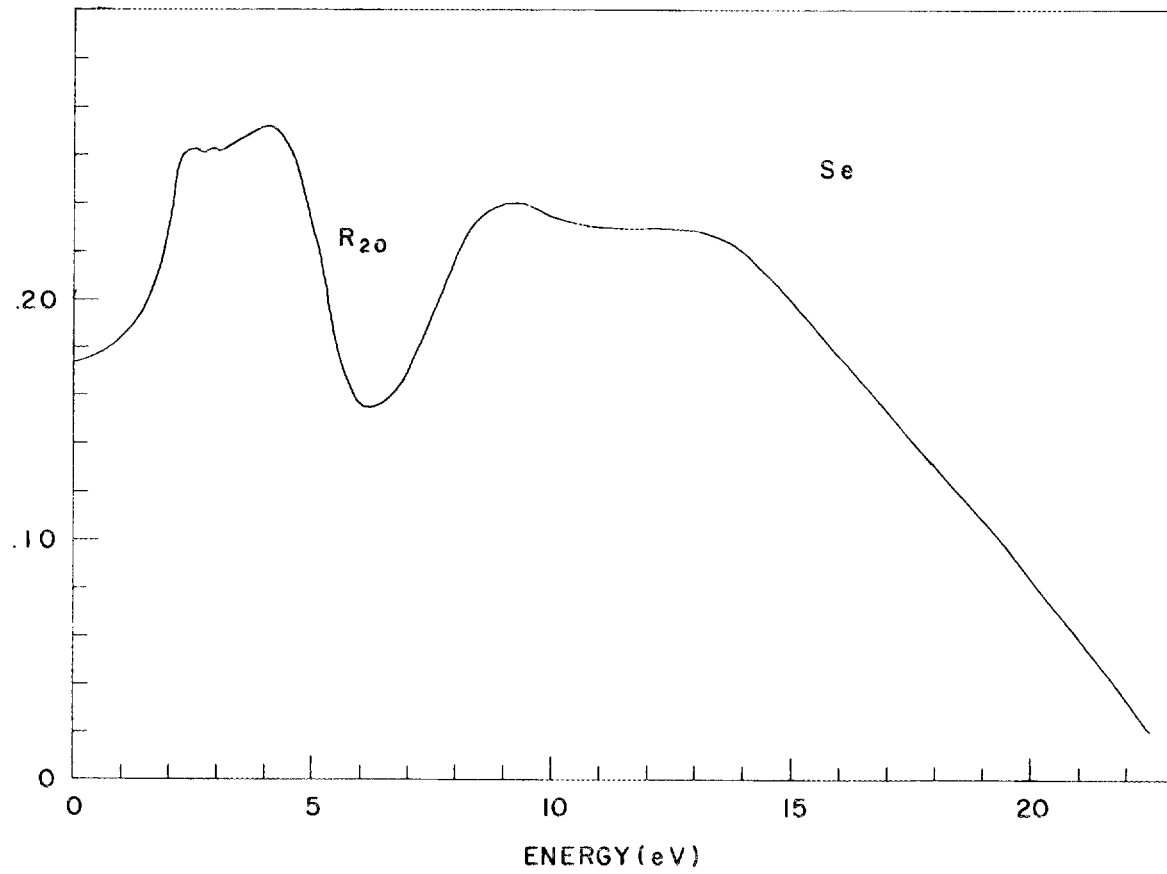


Fig. 7. Input Reflectance for Dispersion Analysis of Selenium.

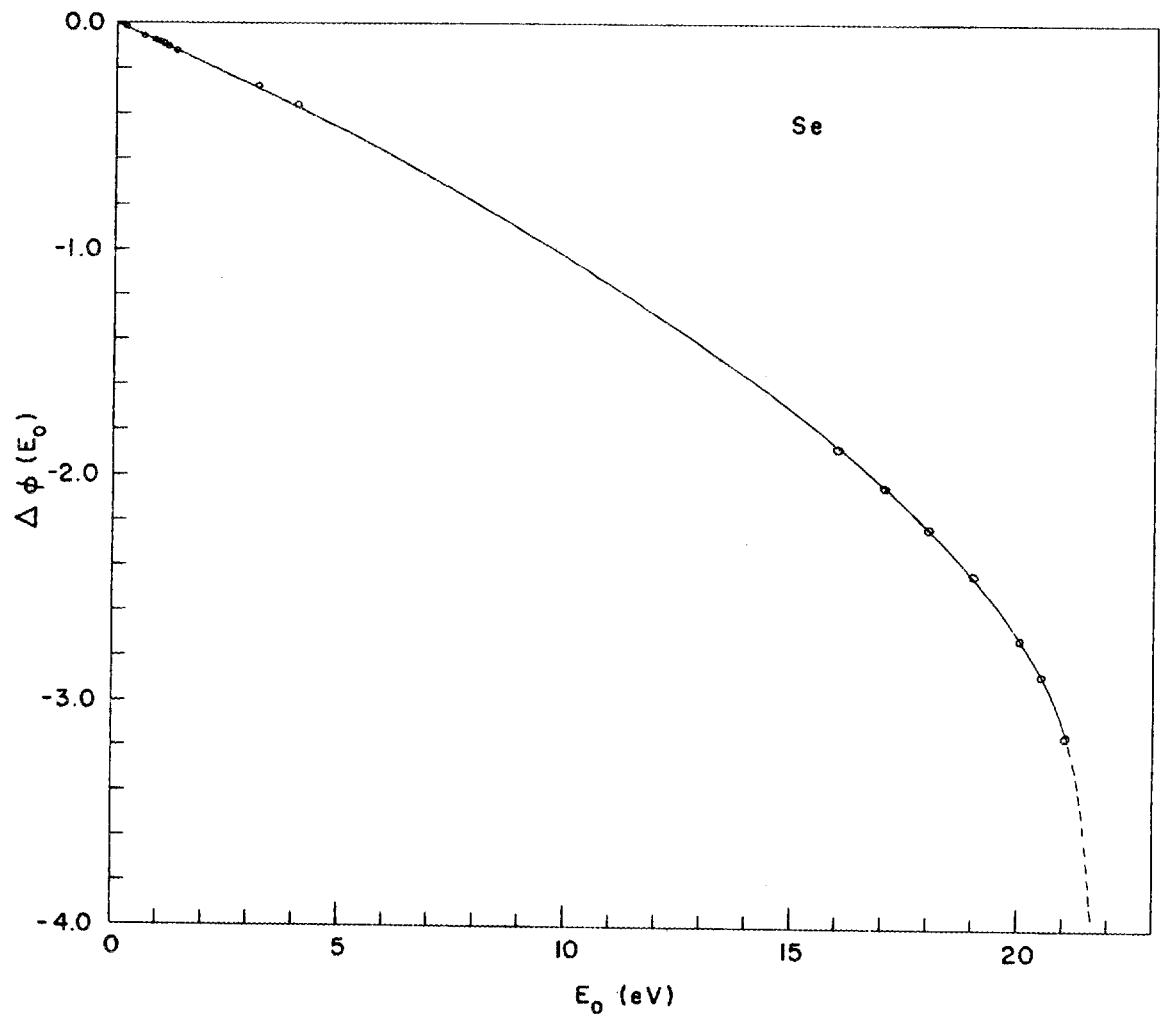


Fig. 8.  $\Delta\phi(E_0)$  versus  $E_0$  for Selenium.

and  $k$  in the energy region 0 to 16 eV using Equations (11) and (12) respectively.

Thus for selenium, the values of  $n$  and  $k$  in the energy region 0 to 16 eV were obtained from the dispersion analysis method, while those above 16 eV were obtained from the two-angle method. These results are shown in Figure 9.

For tellurium the two-angle method gave consistent results between 14 eV and 18 eV but some divergence for energies above 18 eV and below 14 eV. The values of  $n$  in the energy region between 18 eV and 26 eV were obtained from an average of the  $70^\circ$ - $20^\circ$  and the  $70^\circ$ - $45^\circ$  data, while the values of  $k$  in this same energy range were determined from transmission measurements made on films of tellurium evaporated onto thin self-supporting aluminum films as described in Chapter IV. The transmission of the aluminum films measured before the tellurium evaporation was divided into the transmission of the same films after the tellurium evaporation to obtain the transmission,  $T$ , of the tellurium films. Then graphs of  $\log T$  versus thickness of the tellurium films were used to obtain the  $k$  values of tellurium in this energy region. A typical set of these plots is shown in Figure 10.

We were able to obtain values of  $n$  in the energy interval between 28 eV and 40 eV from the critical angle method. The critical angle,  $\theta_m$ , was taken as the angle at which the slope of the reflectance curve was a maximum when the reflectance was plotted versus angle of incidence. The real part of the refractive index was determined using the relation

$$n = \sin \theta_m \quad (18)$$

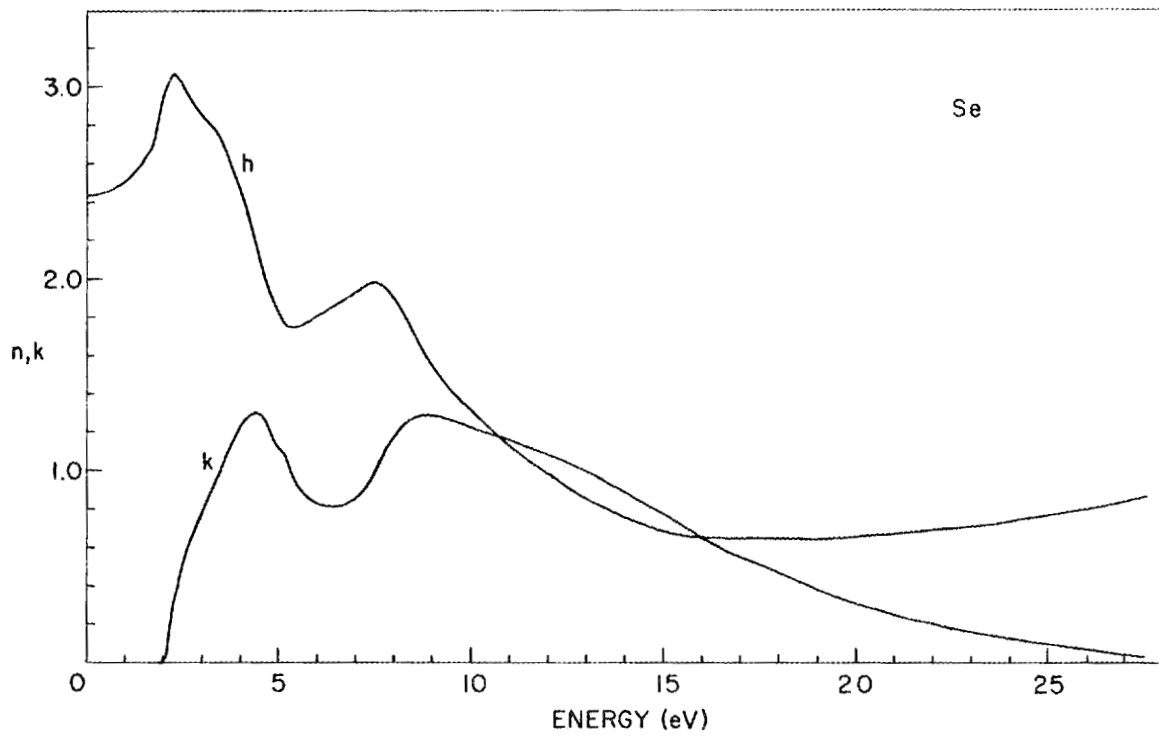


Fig. 9. Optical Constants of Selenium versus Energy.

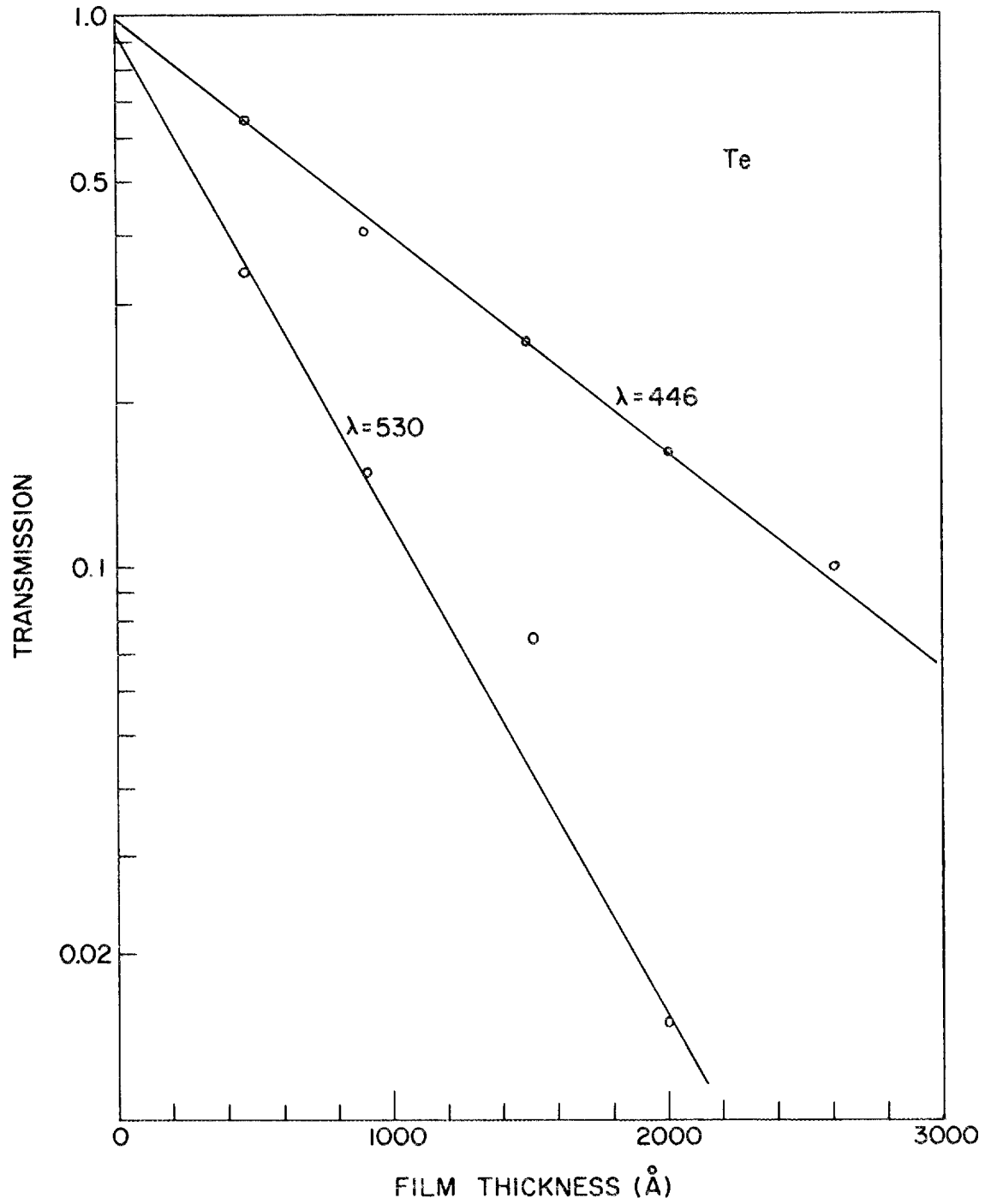


Fig. 10. Transmission of Tellurium Films versus Thickness.

A comparison of the  $n$  and  $k$  values obtained by these methods for the energy region 18 eV to 38 eV is shown in Figure 11.

The values of  $n$  and  $k$  for energies below 14 eV were obtained from a Kramers-Kronig analysis of the reflectance values shown in Figure 12. The reflectance values from 0 to 0.5 eV were calculated from the optical constants determined by Hartig and Loferski<sup>28</sup> for single crystals of tellurium with electric vector of the incident light parallel to the  $c$ -axis of the crystals. The reflectance values in the energy interval 0.5 eV to 3.0 eV were taken from the data of Stuke and Keller<sup>29</sup> for single crystals of tellurium with the electric vector of the incident light parallel to the  $c$ -axis of the crystals. These values best matched our reflectance values on polycrystalline films. The reflectance values from 3 eV to 23 eV were the 20° reflectance values of the present work. The extrapolation used for tellurium was the same type as that used for selenium. The plot of  $\Delta\phi(E_0)$  versus  $E_0$  for tellurium is shown in Figure 13. The final values of  $n$  and  $k$  obtained in this work for tellurium are shown in Figure 14.

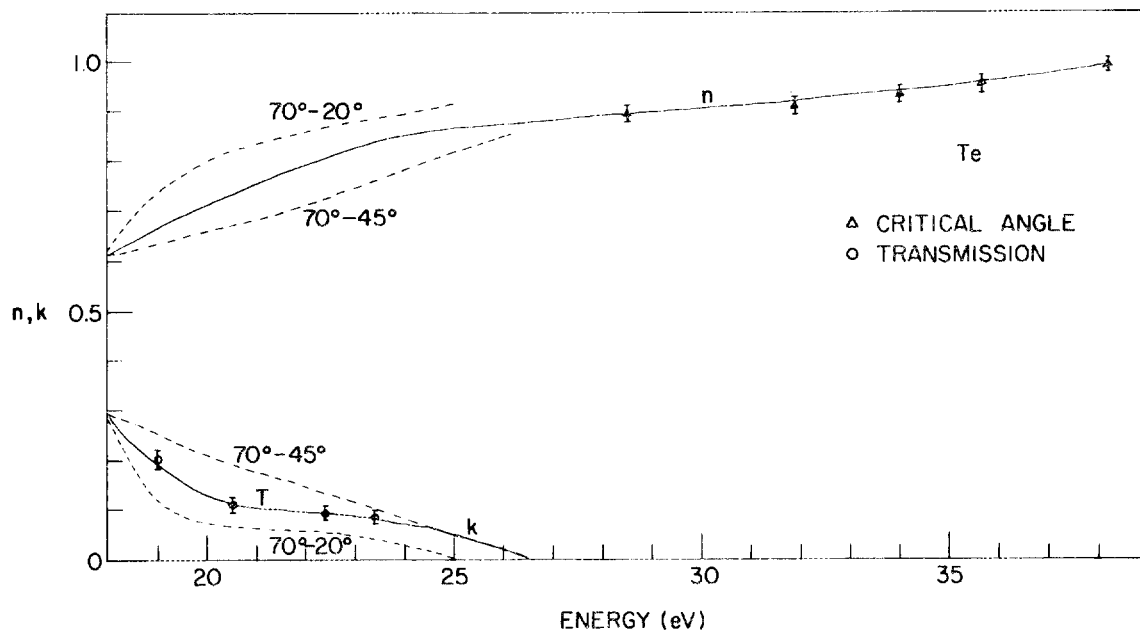


Fig. 11. Comparison of Optical Constants of Tellurium Obtained by the Various Methods Described in the Text.

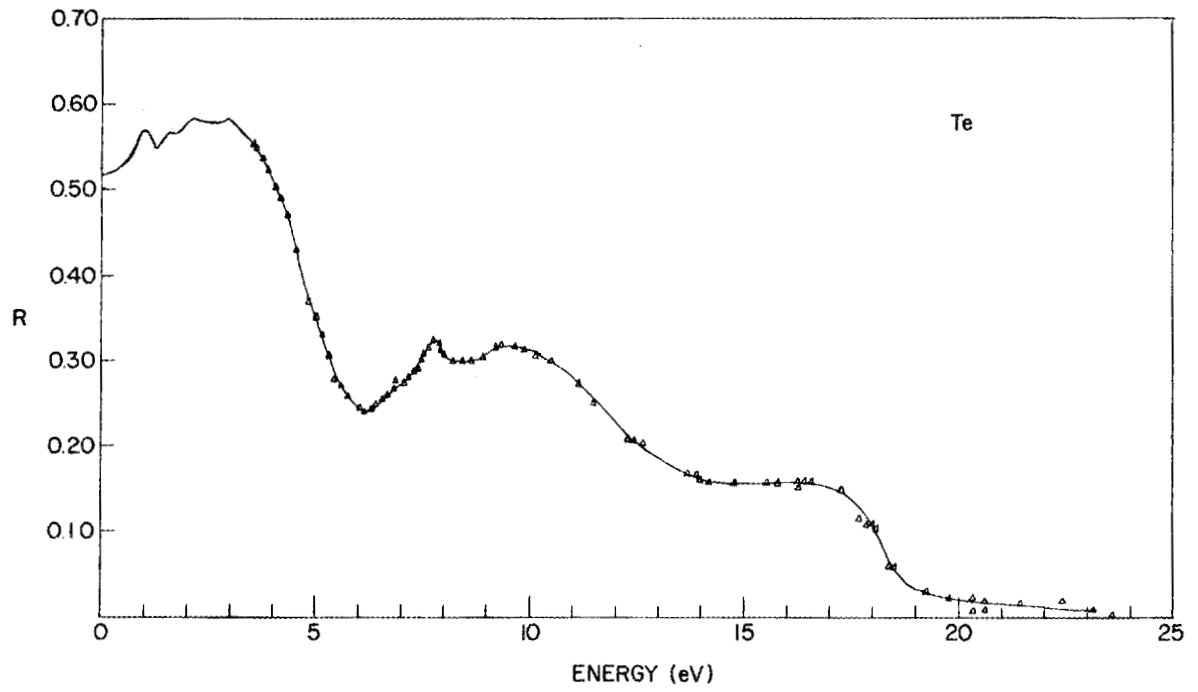


Fig. 12. Input Reflectance for Dispersion Analysis of Tellurium.

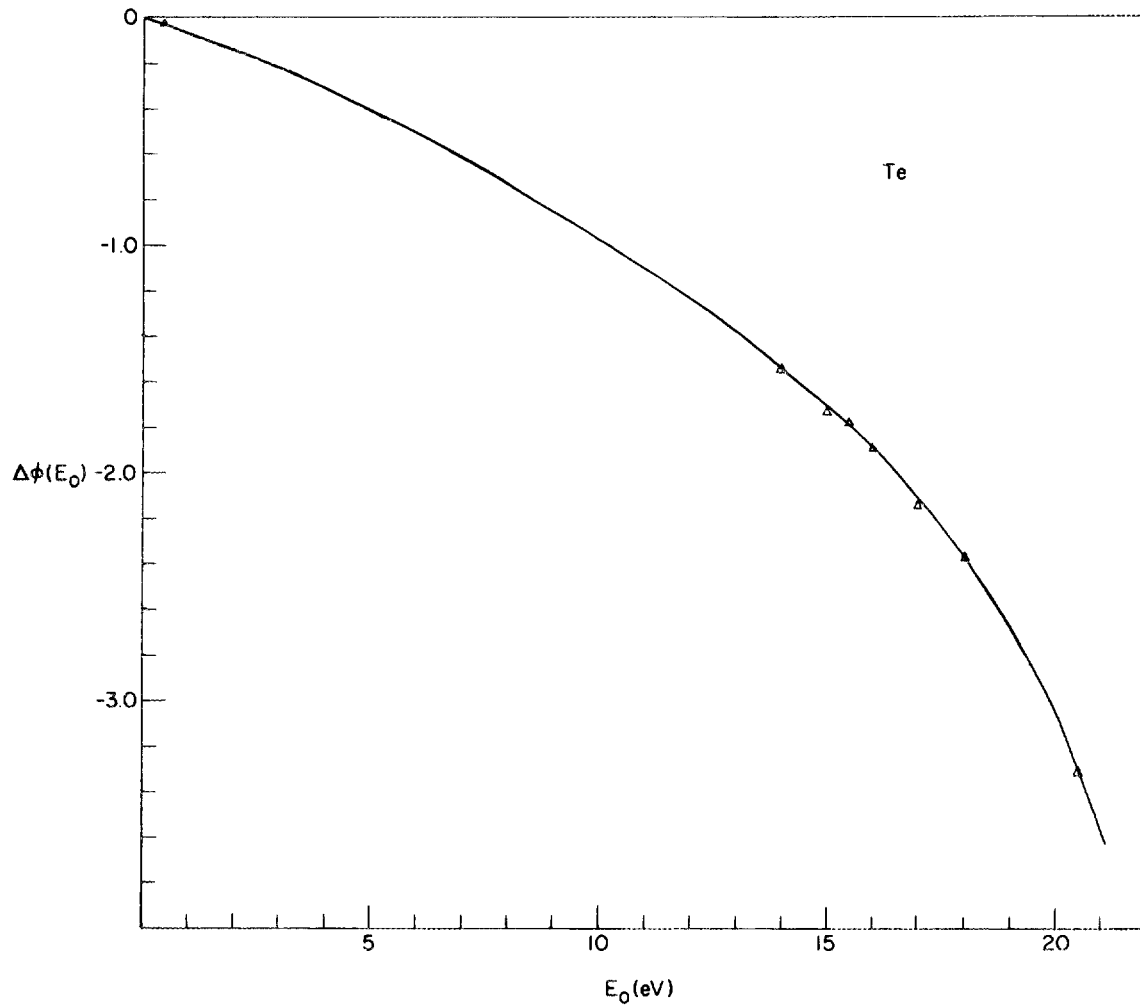


Fig. 13.  $\Delta\phi(E_0)$  versus  $E_0$  for Tellurium.

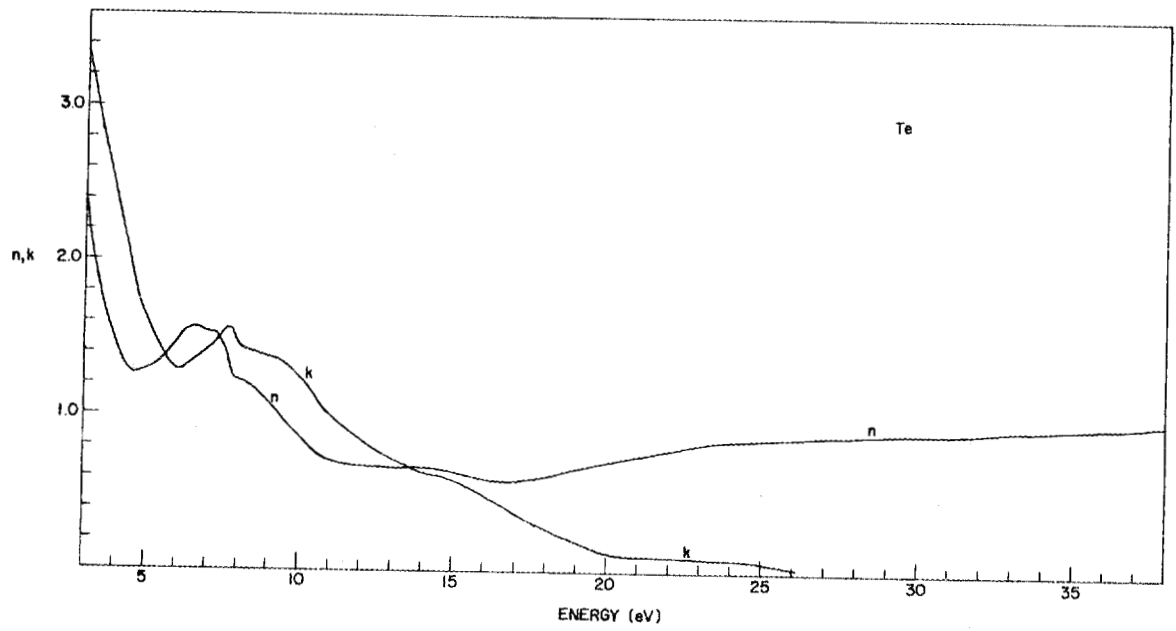


Fig. 14. Optical Constants of Tellurium versus Energy.

## CHAPTER VI

### RESULTS AND CONCLUSIONS

#### A. Selenium

The real and imaginary parts of the complex refractive index,  $N = n + ik$ , are shown graphically in Figure 9. These values represent a composite of values found for a number of evaporated selenium films. The values from 0 to 16 eV were obtained by the dispersion method and the values from 16 eV to 27.5 eV were obtained from the two-angle method. The values above 24.5 eV are based on only a few measurements made at 27.5 eV and contain more uncertainty than the other values. From transmission measurements on selenium Robin-Kandare<sup>4</sup> has measured the absorption coefficient,  $K = \frac{4\pi k}{\lambda}$ , in the spectral region 110 Å to 4000 Å, and has interpreted the results using Reitz's<sup>30</sup> band model. She attributes a set of peaks at about 5 eV to transitions from the second group of p bands to d bands, a maximum at 9 eV to transitions between the first and third groups of p bands and a maximum between 28 and 30 eV to transitions between the 4s band and the conduction band. In the present work, a broad maximum in  $k$  is found at about 9 eV and a small "bump" at about 5 eV. The optical constants up to 5 eV correspond to data previously reported (see Chapter V) and will not be discussed. The values of  $k$  obtained in this work are considerably higher than those measured by Robin-Kandare throughout the vacuum ultraviolet region, except at the 9 eV peak. Robin-Kandare<sup>5</sup> has also measured the 18° reflectance of selenium

up to 12 eV. Her results show a minimum at about 6.5 eV and a peak at 9 eV, but the structure is not as pronounced as that shown in the present results. Vasko<sup>21</sup> has used the dispersion relations relating the real and imaginary parts of the complex refractive index,  $N = n + ik$ , to the absorption coefficient,  $K = \frac{4\pi k}{\lambda}$ , and calculated the constants  $n$  and  $k$  from .13 Å to 150 μ using the absorption coefficient determined by various experimenters including that of Robin-Kandare<sup>5</sup> in the vacuum ultraviolet. His results differ considerably from those of this work in the vacuum ultraviolet spectral region. W. L. Goffe and M. P. Givens<sup>6</sup> have measured the reflectance of selenium in the spectral region 550 Å and 1500 Å. Their values are considerably lower than those reported here. The differences are probably due to the fact that the present measurements were performed on films which had not been exposed to air, since we have found that the reflectance of selenium films exposed to air for a few minutes is considerably less than the reflectance of the same prior to exposure to atmospheric pressure.

The real and imaginary parts of the complex dielectric constant,  $\epsilon(E) = \epsilon_1(E) + i \epsilon_2(E)$ , were calculated from the values of  $n$  and  $k$  and are shown graphically in Figure 15. The optical constant most useful in relating one-electron spectra of solids to band structure is  $\epsilon_2(E)$ .<sup>31</sup> Peaks and sharp edges in  $\epsilon_2(E)$  can be associated with optical transitions which take place in the solid between filled and unfilled states. Since  $\epsilon_2$  is proportional to the joint density of states in the solid, the energy dependence of  $\epsilon_2$  yields information about the relative band gaps in the solid while the shape and magnitude of  $\epsilon_2$  give information about the type and relative importance of the transition.

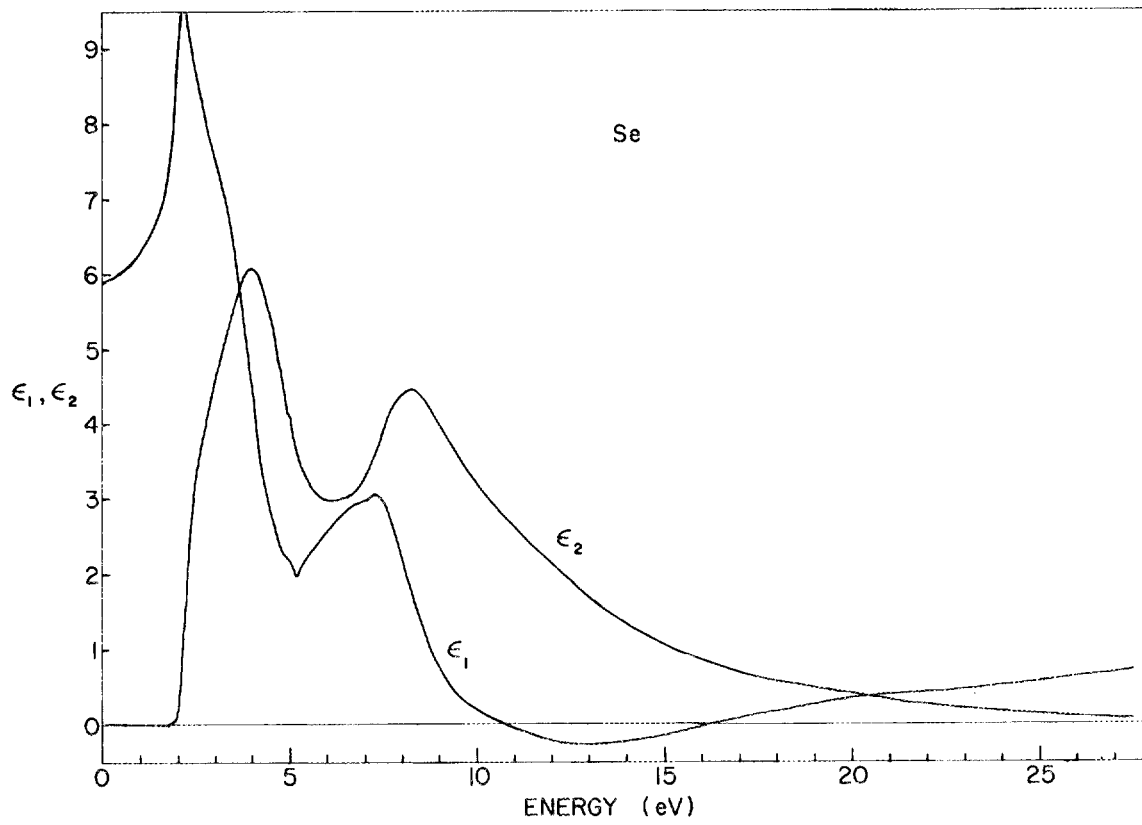


Fig. 15. Dielectric Constants of Selenium versus Energy.

There have been several<sup>30,32,33,34,35</sup> band structure calculations for selenium. The most recent<sup>35</sup> makes use of the molecular-orbital method taking hybridized orbitals as basis functions. Their calculations indicate that the 4s and 4p atomic levels hybridize into 4 levels which are designated as  $\alpha$ ,  $\tau$ ,  $\beta$ , and  $\rho$ . The three lower levels,  $\tau$ ,  $\beta$ , and  $\rho$  are the primary constituents of the valence bands, while the  $\alpha$  and 5s levels make up the major parts of the conduction bands.

For selenium the broad peak in  $\epsilon_2$  beginning at about 7 eV is due to interband transitions, probably from the lower valence levels  $\beta$  and  $\rho$  to the conduction bands. The magnitude of  $\epsilon_2$  at the peak at 8.25 eV is comparable to that of the peak at 4 eV, indicating that the 8.25 eV transition is relatively strong.

The energy-loss functions  $-\text{Im} \frac{1}{\epsilon}$  and  $-\text{Im} \frac{1}{\epsilon+1}$  were calculated from the values of  $n$  and  $k$  and are plotted versus energy in Figure 16. The volume-loss function  $-\text{Im} \frac{1}{\epsilon}$  shows peaks at 5.25 eV and between 18.5 and 19.0 eV, while the surface-loss function,  $-\text{Im} \frac{1}{\epsilon+1}$ , has maxima at 5.25 eV and 14.5 eV. Characteristic-electron-energy losses have been observed in amorphous selenium by Robins<sup>36</sup> who found losses at 5.4 eV, 14.2 eV, 18.8 eV, 37.7 eV, and 55.5 eV. The loss at 14.2 eV was attributed to a surface-plasma loss while the loss at 18.8 eV was attributed to a volume-plasma loss. The loss at 5.4 eV was attributed possibly to an interband transition. The peaks in the energy-loss functions in this work compare well with the measurements of Robins. The loss at 18.8 eV is definitely a volume-plasma loss since  $\epsilon_2$  shows little structure near this energy,  $\epsilon_1$  and  $\epsilon_2$  are small in the region of the peak and approximately linearly varying with  $d\epsilon_1/dE \geq 0$  and  $d\epsilon_2/dE \leq 0$ , while the loss at 14.5 eV is

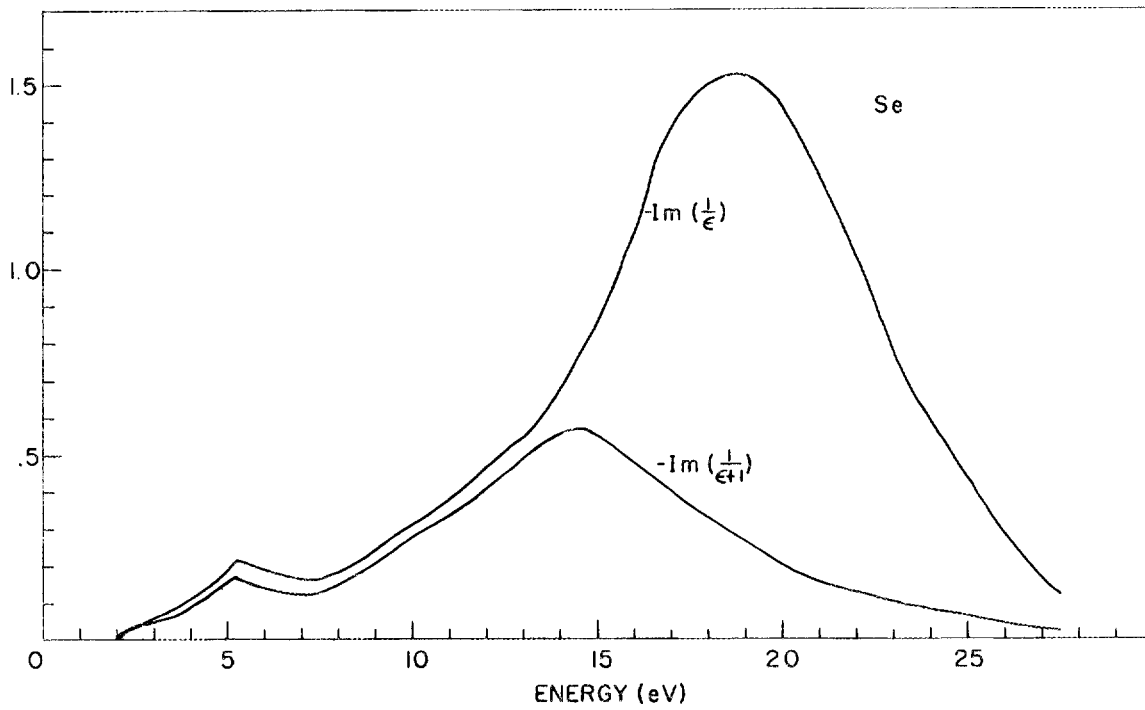


Fig. 16. The Energy Loss Functions of Selenium versus Energy.

definitely a surface-plasma loss since  $\epsilon_2$  shows little structure in this region. We identify the loss near 5.25 eV as due to volume-plasma oscillations involving the electrons in the uppermost valence band.

Selenium has a  $4s^2 4p^4$  electron configuration; therefore one would expect 6 electrons per atom to take part in the major volume-plasma oscillations. Since interband transitions occurring below the plasma energy,  $E_p$ , shift the plasma energy to higher values, the plasma energy will not necessarily be given by the free electron relation,

$$E_p = \hbar \left( \frac{4\pi N e^2}{m} \right)^{\frac{1}{2}} \quad (19)$$

where  $N$  is the number of electrons per unit volume and  $m$  is the electron mass. For six electrons per selenium atom, Equation (19) yields a value of 17.4 eV for the plasma energy. The difference of 1.4 eV between the observed plasma energy and that given by Equation (19) is reasonable since there are strong interband transitions below the expected plasma energy. For two electrons per selenium atom in the top valence band, Equation (19) yields a value of 5.8 eV for the energy associated with collective oscillations involving these electrons. Thus it is reasonable that the loss near 5.25 eV is due to collective oscillations.

#### B. Tellurium

A typical set of reflectance values for polycrystalline tellurium is shown in Figure 17. The near-normal-incidence reflectance of polycrystalline tellurium films on amorphous substrates has been measured by several workers<sup>7,8,9,10</sup> in the energy region above 3 eV. Their values are all significantly lower than the values reported here. We found that

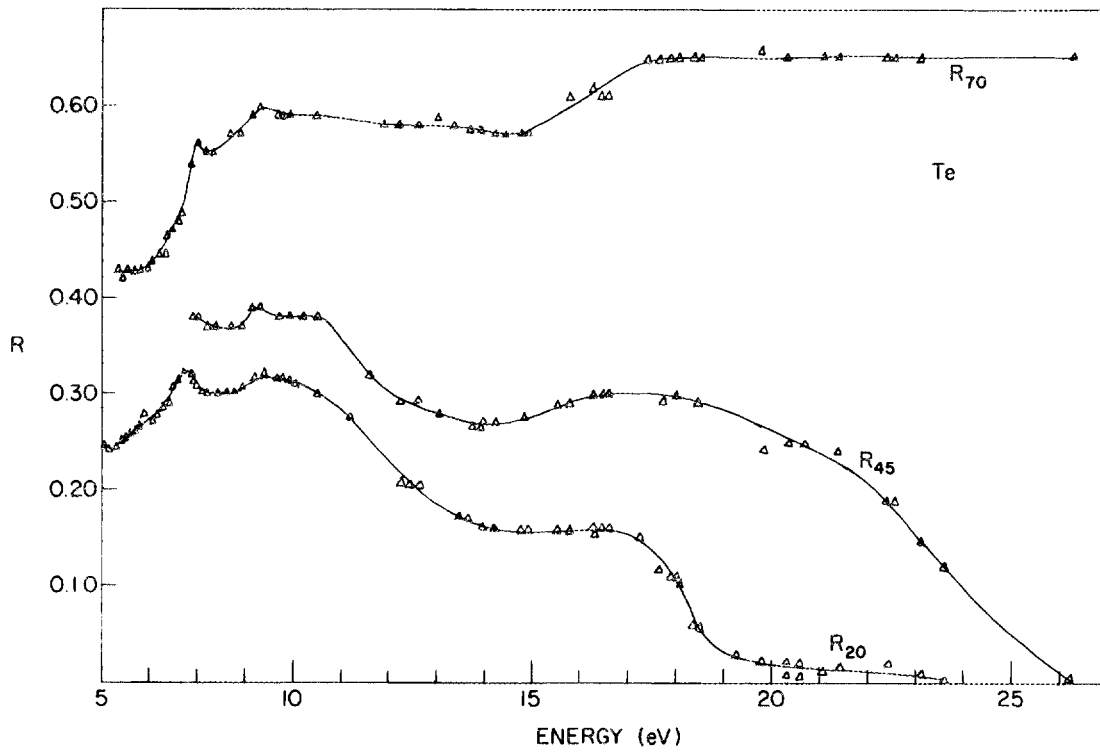


Fig. 17. Reflectance of Vacuum-evaporated Tellurium as a Function of Energy for 20°, 45°, and 75° Angles of Incidence.

exposing the tellurium films to air did not affect the reflectance. The discrepancies in the values reported by the various workers must therefore be due to the condition of the substrates, the speed of the evaporation, or the purity of the sample. Robin-Kandare,<sup>8</sup> Rustgi,<sup>9</sup> and Merdy<sup>10</sup> each observed the peak in the reflectance near 7.8 eV while Merdy<sup>10</sup> and Rustgi<sup>9</sup> each observed the reflectance peak near 9 eV. The plateau in the  $R_{20}$  curve of Figure 17 between 14 eV and 17 eV has not been observed previously. The sharp decrease in reflectance above 17 eV results from the onset of transmission at the plasma frequency. The only other structure which might be noteworthy is a plateau from 20 eV to about 22 eV. Robin-Kandare<sup>4</sup> observed an absorption peak in the energy region 20 to 26 eV for tellurium in transmission measurements. She attributed this edge to transitions from the 5s band to the conduction band (Reitz Model).<sup>30</sup> Our transmission measurements did not show a peak in the energy interval 18 eV to 24 eV (Figure 11). In her transmission measurements Robin-Kandare<sup>8</sup> also observed absorption peaks near 4 eV and near 8 eV.

The real and imaginary parts of the complex refractive index for tellurium for the energy region covered in this experiment are shown in Figure 14. Merdy's<sup>10</sup> paper did not give the constants  $n$  and  $k$ . However, it is possible to obtain them from the real and imaginary parts of the complex dielectric constant using relations (14) and (15). Calculations for a few selected energies indicate that his values for  $n$  and  $k$  were less than those reported here. This is to be expected since his reflectance values for polycrystalline tellurium on amorphous substrates were less than those of the present work.

The real and imaginary parts of the complex dielectric constant were calculated from the values of  $n$  and  $k$  and are shown graphically in Figure 18. In the energy region covered in this work  $\epsilon_2$  has a peak at 7.4 eV and small edges at 8.5 eV and at 9 eV. Several band structure calculations have been made for tellurium.<sup>32,34,37,38,39</sup> All indicate that the band structure of tellurium is very similar to that of selenium. The structure in  $\epsilon_2$  between 7 eV and 9 eV is probably due to interband transitions from levels in tellurium similar to the  $\beta$  and  $\rho$  levels mentioned for selenium to the conduction band.

The energy-loss functions for tellurium are shown in Figure 19. The volume-loss function has peaks at 5.6 eV, 7 eV, 8 eV, and 17.2 eV with a shoulder around 14 eV, while the surface-loss function has peaks at 5.4 eV, 7 eV, 8 eV, and 11.3 eV. Characteristic-electron-energy losses have been observed in tellurium by Möllenstedt,<sup>40</sup> Leder and Marton,<sup>41</sup> Gauthé<sup>42</sup> and Robins.<sup>36</sup> Robins observed losses at 5.2 eV, 11.8 eV, 17.0 eV, 29.1 eV, 33.8 eV, 41.5 eV, and 50.5 eV. The loss at 5.2 eV was attributed possibly to interband transitions, while the loss at 11.8 eV was attributed to surface-plasma oscillations and the loss at 17.0 eV to volume-plasma oscillations. The peaks in the energy-loss functions of the present work agree well with the losses observed by Robins. We associate the 5.6 eV peak with the loss observed by Robins at 5.4 eV and attribute this loss to volume-plasma oscillations involving the electrons in the uppermost valence band. The 11.3 eV peak in the surface-loss function is associated with surface-plasma oscillations while the 17.2 eV peak corresponds to volume-plasma oscillations of all the valence electrons. The shoulder in the volume-loss function near 14 eV is due to

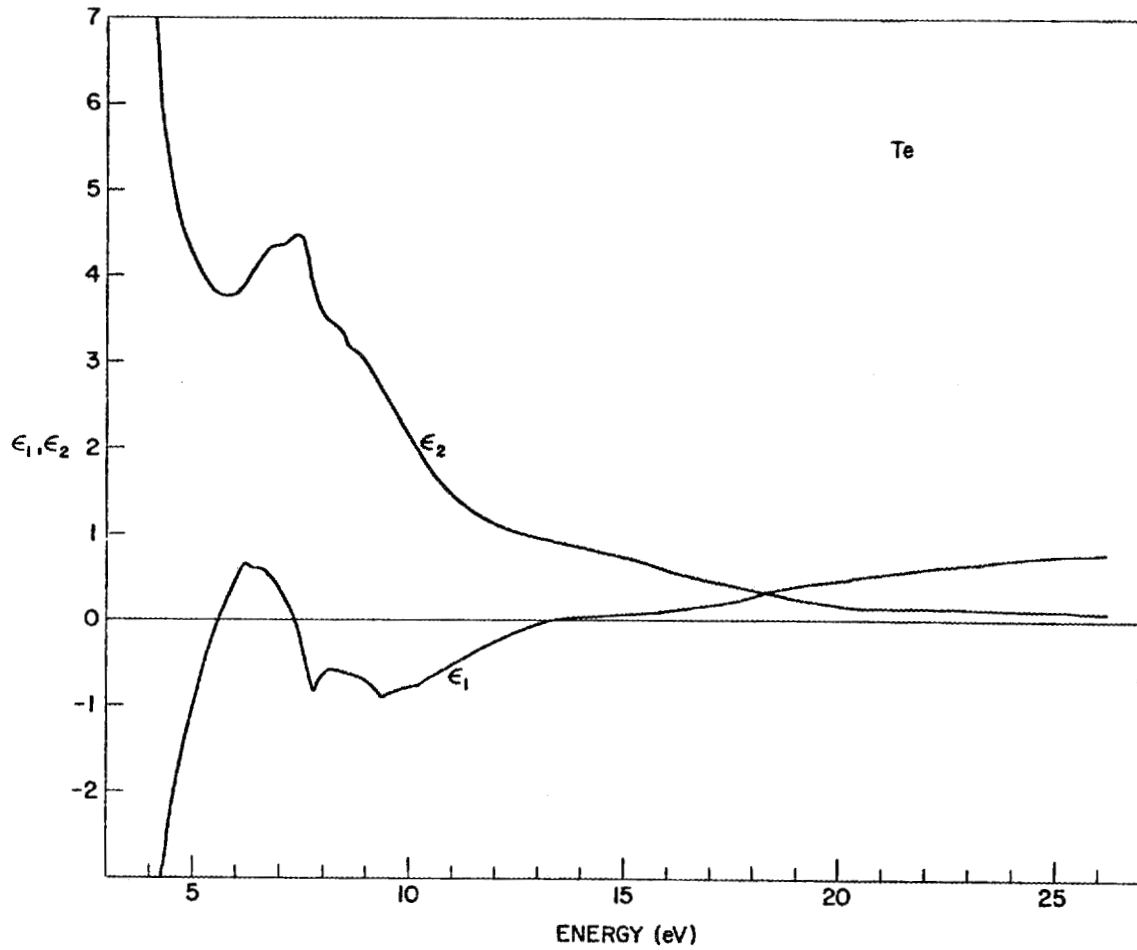


Fig. 18. Dielectric Constants of Tellurium versus Energy.

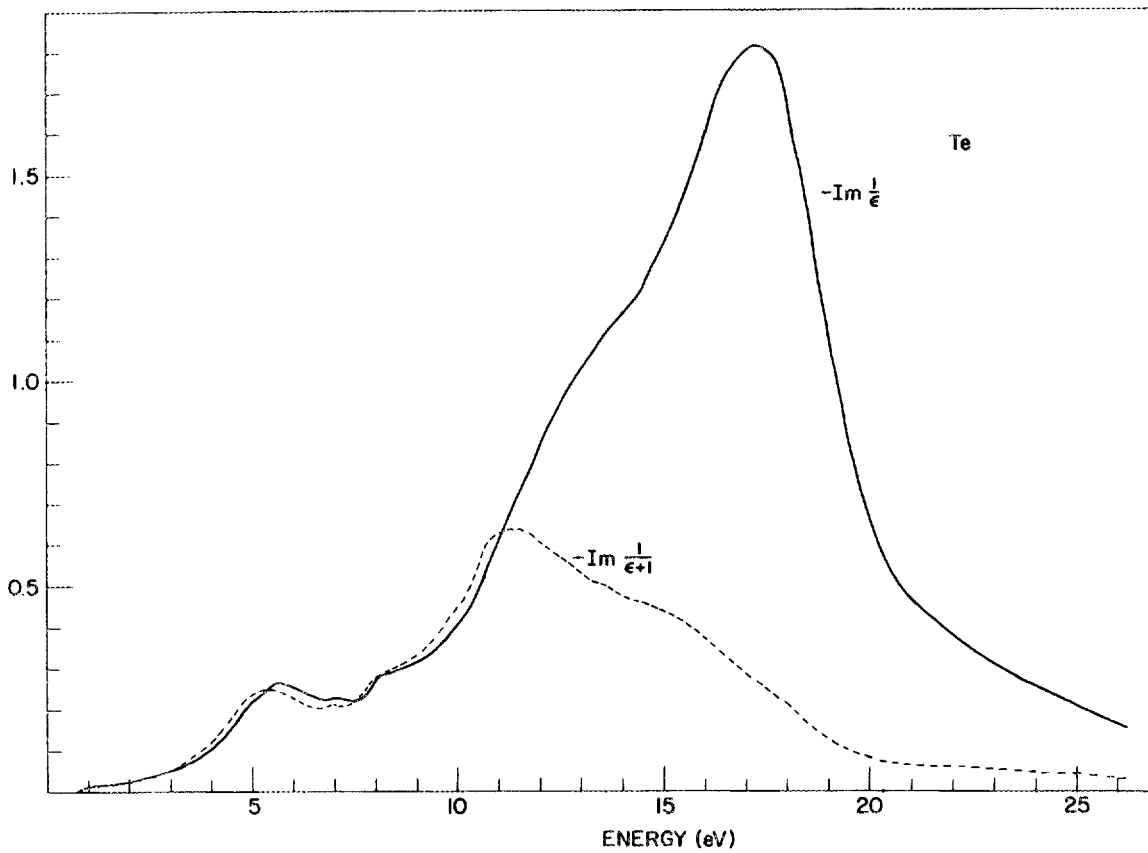


Fig. 19. The Energy Loss Functions of Tellurium versus Energy.

the fact that  $\epsilon_1$  goes through zero in this energy region. There may be volume-plasma oscillations associated with this structure, also.

For 6 electrons per tellurium atom Equation (19) yields a theoretical plasma energy of 15 eV. The difference of 2.2 eV between the theoretical value and the observed value is reasonable since there are strong interband transitions fairly close in energy to the expected plasma energy. For 2 electrons per tellurium atom Equation (19) yields a value of 5 eV which is reasonably close to the peak in the volume-loss function at 5.6 eV.

From this work we have found that the optical properties of evaporated films of tellurium and amorphous selenium are very similar. Both materials have a strong absorption band around 8 eV and both materials can have volume-plasma oscillations at two different energies, between 5 and 6 eV and between 17 and 19 eV.

We have found that it is possible to prepare evaporated tellurium films with reflectance comparable to that of tellurium single crystals and that the reflectance of these films does not seem to be affected by exposure to air. However, amorphous selenium films do show a considerable decrease in reflectance upon exposure to air. These findings indicate that the reflectance values at low energies reported earlier for these substances may be too low.

## BIBLIOGRAPHY

1. F. C. Jahoda, Phys. Rev. 107 (1957).
2. F. Stern, Solid State Physics (ed. F. Seitz and D. Turnbull) 15, 299 (1963).
3. W. R. Hunter, J. Opt. Soc. Am. 54, 15 (1964).
4. S. Robin-Kandare, J. Phys. Radium 21, 31 (1960).
5. S. Robin-Kandare, C. R. Acad. Sci. (Paris) 244, 571 (1957).
6. W. L. Goffe and M. P. Givens, J. Opt. Soc. Am. 53, 804 (1963).
7. G. B. Sabine, Phys. Rev. 55, 1064 (1939).
8. S. Robin-Kandare, Thesis (Paris), (1959).
9. O. P. Rustgi, W. C. Walker, and G. L. Weissler, J. Opt. Soc. Am. 51, 1357 (1951).
10. Henry Merdy, Ann. Phys. (Paris) 1 (5-6), 289 (1966).
11. A. Vasicek, Optics of Thin Films (North-Holland Publishing Company, Amsterdam, 1960).
12. M. Born and E. Wolf, Principles of Optics (Pergamon Press, New York, 1959).
13. T. S. Moss, Optical Properties of Semiconductors (Butterworth & Co., London, 1961).
14. R. N. Hamm, R. A. MacRae, and E. T. Arakawa, J. Opt. Soc. Am. 55, 1460 (1965).
15. United Mineral and Chemical Corporation, 129 Hudson Street, New York.

16. Distributed by Seebee Paint and Chemical Co. 4627 West 60th Street, Chicago 29, Illinois.
17. L. R. Canfield, G. Hass, and W. R. Hunter, *J. Phys. Radium* 25, 124 (1964).
18. Victawet 35B, Obtained from Victor Chemical Works, Chicago, Illinois.
19. K. Ishiguro and T. Sasaki, *J. Appl. Phys. (Japan)* 2, 289 (1963).
20. W. R. Hunter, *J. Opt. Soc. Am.* 55, 1197 (1965).
21. A. Vasko, *Czech. J. Phys.* B15, 170 (1965).
22. R. S. Caldwell and H. Y. Fan, *Phys. Rev.* 114, 664 (1959).
23. W. F. Koehler, F. K. Odencrantz and W. C. White, *J. Opt. Soc. Am.* 49, 109 (1959).
24. H. R. Phillip and E. A. Taft, *Phys. Rev.* 136, A1445 (1964).
25. D. M. Roessler, *Brit. J. App. Phys.* 6, 1119 (1965).
26. H. Ehrenreich, H. R. Phillip and B. Segall, *Phys. Rev.* 132, 1918 (1963).
27. R. A. MacRae, E. T. Arakawa and M. W. Williams, "Optical Properties of Vacuum-evaporated White Tin," *Phys. Rev.* (to be published).
28. P. A. Hartig and J. J. Loferski, *J. Opt. Soc. Am.* 44, 17 (1954).
29. J. Stuke and H. Keller, *Phys. Stat. Sol.* 7, 189 (1964).
30. J. R. Reitz, *Phys. Rev.* 105, 1233 (1957).
31. J. C. Phillips, *Solid State Physics* (ed. F. Seitz and D. Turnbull) 18, 55 (1966).
32. R. Gaspon, *Acta. Phys. Hung.* 7, 289 (1957).
33. D. J. Olechna and R. S. Knox, *Phys. Rev.* 140, A986 (1965).
34. J. Treusch and R. Sandrock, *Phys. Stat. Sol.* 16, 487 (1966).

35. S. Tutihasi and I. Chen, Phys. Rev. (to be published).
36. J. L. Robins, Proc. Phys. Soc. (London) 79, 119 (1962).
37. R. E. Beissner, Phys. Rev. 145, 479 (1966).
38. M. Hulin, J. Phys. Chem. Solids 27, 441 (1966).
39. A. Nussbaum and R. J. Hager, Phys. Rev. 123, 1958 (1961).
40. G. Möllenstedt, Optik (Stuttgart) 5, 499 (1949).
41. L. B. Leder and L. Marton, Phys. Rev. 95, 1345 (1954).
42. B. Gauthe, Phys. Rev. 114, 1265 (1959).

## DISTRIBUTION FOR ORNL-TM-2023

### INTERNAL DISTRIBUTION

- |   |                                  |
|---|----------------------------------|
| 1. Biology Library  | 101. H. G. MacPherson            |
| 2-4. Central Research Library                                   | 102. W. J. McConnell             |
| 5. Reactor Division Library                                     | 103. K. Z. Morgan                |
| 6-7. ORNL-Y-12 Technical Library,<br>Document Reference Section | 104. R. H. Ritchie               |
| 8-57. Laboratory Records Department                             | 105. H. C. Schweinler            |
| 58. Laboratory Records, ORNL R.C.                               | 106. M. J. Skinner               |
| 59-83. E. T. Arakawa  | 107. R. C. Vehse                 |
| 84-94. R. D. Birkhoff   | 108. A. M. Weinberg              |
| 95. J. G. Carter  | 109. J. C. Frye (consultant)     |
| 96. L. C. Emerson   | 110. G. M. Fair (consultant)     |
| 97. R. N. Hamm  | 111. J. B. Hursh (consultant)    |
| 98. H. H. Hubbell, Jr.  | 112. R. L. Platzman (consultant) |
| 99. W. H. Jordan  | 113. E. P. Odom (consultant)     |
| 100. C. E. Larson   | 114. H. O. Wyckoff (consultant)  |

### EXTERNAL DISTRIBUTION

115. F. Abeles, Institut d'Optique, Paris, France
116. H. C. Allison, University of Tennessee, Martin Branch, Martin, Tennessee
117. N. Axelrod, Bell Laboratories, Murray Hill, New Jersey
118. N. F. Barr, Division of Biology and Medicine, USAEC, Washington, D.C.
119. M. J. Berger, National Bureau of Standards, Division 403, Washington, D.C.
120. C. N. Berglund, Bell Laboratories, Murray Hill, New Jersey
121. H. Boersch, I. Physikalisches Institut der Technischen Universität, Berlin, Germany
122. R. M. Chaduhri, High Tension and Nuclear Research Laboratory, Church Road, Government College, P. O. Box 701, Lahore, W. Pakistan
123. J. R. Cuthill, Alloy Physics Section, National Bureau of Standards, Washington, D.C.
124. J. P. Davey, Cambridge University, Department of Physics, Cavendish Laboratory, Cambridge, England
125. W. D. Deeds, Department of Physics, University of Tennessee, Knoxville, Tennessee
126. H. Ehrenreich, Physics Department, Harvard University, Cambridge, Massachusetts
127. Mlle. D. Fabre, CNRS, Laboratoire de Bellevue, Bellevue, France
128. U. Fano, National Bureau of Standards, Washington, D.C.
129. R. A. Ferrell, Physics Department, University of Maryland, College Park, Maryland.
130. H. A. Fowler, Electron Physics Section, National Bureau of Standards, Washington, D.C.
131. F. W. Garber, Physics Department, University of Tennessee, Knoxville, Tennessee
132. D. C. Hammer, NASA, Lewis Research Center, Cleveland, Ohio

133. W. F. Hanson, Physics Department, University of Tennessee, Knoxville, Tennessee
134. E. G. Harris, Physics Department, University of Tennessee, Knoxville, Tennessee
- 135-145. J. D. Hayes, 3402 Cavanaugh Drive, Huntsville, Alabama 35810
146. A. Heiser, Department of Physics, Vanderbilt University, Nashville, Tennessee
147. R. J. Herickhoff, Mankato State College, Mankato, Minnesota
148. R. H. Huebner, Physics Department, University of Tennessee, Knoxville, Tennessee
149. W. R. Hunter, U. S. Naval Research Laboratory, Washington, D.C.
150. G. S. Hurst, Physics Department, University of Kentucky, Lexington, Kentucky
151. T. M. Jelinek, Space Nuclear Propulsion Office, Lewis Research Center, 2100 Brookpark Road, Cleveland, Ohio
152. W. C. H. Joiner, Westinghouse Electric-Aerospace Division, Box 746, Baltimore, Maryland
153. H. Kanter, Aerospace Corporation, Box 95085, Los Angeles 45, Calif.
154. S. A. Lough, Division of Biology and Medicine, USAEC, Washington, D.C.
155. R. A. MacRae, Physics Department, Jacksonville State University, Jacksonville, Alabama 36265
156. R. P. Madden, National Bureau of Standards, Washington 25, D.C.
157. L. Marton, National Bureau of Standards, 4515 Linnean Avenue, S.W., Washington, D.C.
158. H. Mayer, Physikalisches Institut des Technischen Hochschule, Clausthal, Germany
159. H. Mendlowitz, National Bureau of Standards, Atomic Physics Division, Washington, D.C.
160. K. P. Miyake, Institute for Optical Research, Kyoiku University, Tokyo, Japan
161. M. Y. Nakai, Osaka Laboratory, JAERI, 508 Mii, Neyagawa-City, Osaka, Japan
162. A. H. Nielsen, Department of Physics, University of Tennessee, Knoxville, Tennessee
163. A. Otto, II, Physikalisches Institut der Universitat Munchen, Munchen, 13, Germany
164. H. R. Philipp, General Electric Research Laboratory, P.O. Box 1088, Schenectady, New York
165. J. F. Pierce, Electrical Engineering Department, University of Tennessee, Knoxville, Tennessee
166. C. J. Powell, National Bureau of Standards, Washington, D.C.
167. H. L. Pray, Arkansas State Teacher's College, Conway, Arkansas
168. O. P. Rustgi, Electromagnetics Lab. Research Department, Northrup Space Laboratories, 1111 E. Broadway, Hawthorne, California

169. S. Robin, Faculte des Sciences, L'Universite de Dakar, Sengal, French West Africa
170. J. L. Robins, Cornell University, Ithaca, New York
171. P. Rouard, Faculte des Sciences, Laboratoire de Physique General, Marseille, France.
172. T. Sasaki, College of General Education, University of Tokyo, Komaba, Tokyo, Japan
173. G. Sauerbrey, Physikalisch-Technische Bundesanstalt, Berlin-Charlottenburg, Germany
174. A. N. Saxena, Fairchile Semiconductor, 4110 Junipero Sera Blvd., Palo Alto, California
175. J. A. Simpson, National Bureau of Standards, 312 Riley Street, Falls Church, Virginia
176. W. E. Spicer, Stanford Electronics Laboratory, Stanford University, Stanford, California
177. W. Steinman, II. Physikalisches Institute der Universitat Munchen, Munchen 13, Germany
178. E. A. Stern, University of Maryland, Department of Physics, College Park, Maryland
179. J. B. Swan, Department of Physics, University of Western Australia, Nedlands, Western Australia
180. Nils Swanson, National Bureau of Standards, West 103, Washington 25, D. C.
181. E. A. Taft, General Electric Research Laboratory, P. O. Box 1088, Schenectady, New York
182. Ye-Yung Teng, Department of Physics and Astronomy, University of Maryland, College Park, Maryland
183. J. Thomas, Department of Public Health, Yale University, New Haven, Connecticut
184. G. L. Weissler, University of Southern California, Department of Physics, Los Angeles, California
185. P. R. Wessel, U. S. Naval Ordnance Laboratory, Silverspring, Maryland
186. S. Yamaguchi, Department of Physics, Tokyo Metropolitan University, Setagaya-Ku, Tokyo, Japan
187. V. B. Bohnot, Physics Department, Panjab University, Chandigarh-3, India
188. Jacobo Rapaport, University of Chile, Box 277, Institute of Science, Santiago, Chile
189. Research and Development Division, AEC, ORO
190. J. O. Thomson, Physics Department, University of Tennessee, Knoxville, Tennessee
191. F. T. Wooten, Lawrence Radiation Laboratory, University of California, Berkeley, California
- 192-206. Division of Technical Information Extension.

